Molecular layer interneurons in the cerebellum encode for valence in associative learning

Ming Ma[1,2], Gregory L. Futia[3], Fabio M. Simoes De Souza[2,4], Baris N. Ozbay[5], Isabel Llano[6], Emily A. Gibson[1,3] and Diego Restrepo[1,2,*]

[1]Neuroscience Graduate Program, University of Colorado Anschutz Medical Campus, Aurora, CO 80045, USA

[2]Department of Cell and Developmental Biology, University of Colorado Anschutz Medical Campus, Aurora, CO 80045, USA

[3]Department of Bioengineering, University of Colorado Anschutz Medical Campus, Aurora, CO 80045, USA

[4]Center for Mathematics, Computation and Cognition, Federal University of ABC, Sao Bernardo do Campo, SP, Brazil.

[5]Intelligent Imaging Innovations, Denver, CO, 80216.

[6]Saints Pères Paris Institute for Neurosciences, Université Paris Descartes, 75006 Paris, France

[*]Corresponding author: Diego Restrepo, diego.restrepo@cuanschutz.edu

We used two-photon microscopy to study the role of ensembles of cerebellar molecular layer interneurons (MLIs) in a go-no go task where mice obtain a sugar water reward if they lick a spout in the presence of the rewarded odorant and avoid a time out when they refrain from licking for the unrewarded odorant. In naïve animals the MLI responses did not differ between the odorants. With learning, the rewarded odorant elicited a large increase in MLI calcium responses, and the identity of the odorant could be decoded from the differential response. Importantly, MLIs switched odorant responses when the valence of the stimuli was reversed. Finally, mice took a longer time to refrain from licking in the presence of the unrewarded odorant and had difficulty becoming proficient when MLIs were inhibited by chemogenetic intervention. Our findings support a role for MLIs in learning valence in the cerebellum.

36 The cerebellum plays a pivotal role in coordinating movements through sensorimotor
37 integration. It receives massive input through mossy fiber (MF) synapses onto granule cells
38 (GCs) to form a circuit efficient in complex pattern separation[1] (Supplementary Fig. 1). In
39 addition, the cerebellum contributes to cognition and emotion and is associated with non-
40 motor conditions such as autism spectrum disorders[2-5]. The Purkinje cells (PCs), the sole
41 projection neurons of the cerebellar cortex, receive excitatory afferent input from the
42 parallel fibers (PFs) of GCs and dense feedforward inhibitory inputs from the molecular
43 layer interneurons (MLIs). Importantly, subtle changes in this PC excitatory-inhibitory
44 balance generate robust, bidirectional changes in the output of PCs[6].
45
46 Plasticity in cerebellar circuit activity plays an important role in generation of adequate
47 output. Indeed, long term depression (LTD) mediated by dendritic increases in Ca^{2+} in PCs
48 elicited by motor error signals conveyed by climbing fibers (CFs) is a classical model of
49 plasticity[7-10]. However, recent studies indicate that CFs also signal reward prediction[11,12]
50 or decision-making errors[13], and the cerebellum modulates association pathways in the
51 ventral tegmental area (VTA) contributing to reward-based learning and social behavior[14].
52 Furthermore, although LTD at the PF-PC synapse is often considered as the substrate for
53 cerebellar dependent learning[7-10], such learning can occur in the absence of LTD and may
54 therefore involve other forms of plasticity[15]. A potential substrate for plasticity is the PF-
55 MLI synapse[16,17] where LTP can be induced in slices by pairing MLI depolarization with
56 PF stimulation[18] and *in vivo* by conjunctive stimulation of PFs and CFs[19], believed to
57 underlie changes in the size of cutaneous receptive fields[20,21]. Additionally, high frequency
58 stimulation of PFs alters subunit composition of AMPA receptors, rendering them calcium-

59 impermeable[18], a long-lasting change linked to behavioral modifications[22]. Interestingly,
60 MLIs have been proposed to participate in cerebellar plasticity[21,23,24], and Rowan and co-
61 workers found graded control of PC plasticity by MLI inhibition[25] suggesting that MLI
62 inhibition is a gate for learning stimulus valence which conveys information as to whether
63 the stimulus is rewarded. However, whether there is a causal participation of MLIs in
64 reward-associated learning is unknown.
65
66 Here we explored whether MLI activity plays a role in reward-associated learning in a go-
67 no go task where the thirsty animal learns to lick to obtain a water reward[26,27]. We applied
68 two-photon microscopy[28] to record Ca^{2+} changes in ensembles of MLIs and utilized
69 chemogenetics to explore the functional role of MLI activity in learning.
70
71

72 **Results**

73

74 In order to explore the role of MLIs in associative learning we employed *in vivo* two-photon
75 microscopy to record neural activity reported by changes in fluorescence emitted by the
76 Ca^{2+} indicators GCaMP6/7. MLIs were imaged within the superficial 50 μm of the ML in
77 head-fixed mice through a 2x2 mm glass window implanted above the cerebellar vermis
78 (lobule VI, Fig. 1, Supplementary Fig. 2), where GCs acquire a predictive feedback signal
79 or expectation reward[29,30]. We used the go-no go task where thirsty mice initiate the trial
80 by licking on the spout to elicit odorant delivery 1-1.5 sec after the first lick. Mice received
81 a water reward when they licked at least once in two lick segments during rewarded odorant
82 delivery (1% isoamyl acetate, Iso, termed S+) (Fig. 1a, Hit trial, mouse movement shown
83 in Supplementary Movie 1, quantified in Supplementary Fig. 3). Mice did not receive the
84 reward if they failed to lick in one of the two lick segments (Miss trial). When the
85 unrewarded odorant was presented (mineral oil, MO, S- trials) the animals did not receive
86 a reward when they refrained from licking (Correct Rejection, CR, Fig. 1a), and they
87 received a timeout of ten seconds if they licked in both segments (False Alarm, FA). A
88 proficient mouse (percent correct>=80%) licked at least once in each lick segment in the
89 S+ trials and stopped licking during the segments for the S- trials, see lick trace at the
90 bottom of Fig. 1d.

91

92 An example of an increase in MLI GCaMP6f fluorescence intensity during odorant
93 application in a Hit trial is shown for a proficient mouse in Figs. 1bi,ii (Supplementary
94 Movie 2). We extracted regions of interest (ROIs) of the components (Fig. 1biii) and

95 temporal traces of the normalized change in fluorescence (ΔF/F, Figs. 1c and d) using
96 constrained nonnegative matrix factorization analysis[31]. The average diameter of the ROIs
97 in this field of view (FOV) was 10.5±4 μm (mean±SD, n=170, Supplementary Fig. 4a),
98 which falls within the range of diameters reported for MLIs[32]. When the animal was
99 proficient we observed that MLI ΔF/Fs increased when the rewarded odorant was presented
100 (Fig. 1ci and d, vertical orange lines in 1d indicate odorant on and off times for S+). In
101 contrast, the unrewarded odorant elicited smaller transient increases in ΔF/F (Fig. 1cii, Fig.
102 1d vertical light blue lines and Supplementary Figs. 4b,c,d), with some exceptions where
103 the increases for ΔF/F for S- were larger (arrow in Fig. 1d). Finally, the rewarded odorant
104 elicited increases in ΔF/F in 89% of the ROIs among a total of 191 (Fig. 1c and
105 Supplementary Figs. 4c and d).
106
107 **Cerebellar MLIs develop divergent responses as mice learn to differentiate odorants.**
108 The behavioral performance in a learning session where the animal reached proficient level
109 after 70 trials is shown in Fig. 2a. When the animal was naïve (<=65% correct) the time
110 courses for ΔF/F overlapped between S+ and S- (Fig. 2bi), and when the animal became
111 proficient the time courses for ΔF/F diverged (Fig. 2biii). For the proficient animal in S+
112 trials ΔF/F started increasing at trial initiation (1-1.5 sec before odorant addition) and
113 reached a peak when the animal was rewarded (Fig. 2biii, orange trace), while for S- trials,
114 the response returned to basal levels shortly after the odorant was applied (Fig. 2biii, light
115 blue trace, Fig. 2b shows the time courses for lick rates). Whereas ΔF/F does not differ
116 between S+ and S- before odorant addition (Fig. 2c), it diverges after odorant addition as
117 the animal learns (Fig. 2d) and ΔF/F per ROI increased when the animal became proficient

118 (Fig. 2e). GLM analysis yields a statistically significant difference between S+ and S- and
119 naïve and proficient, $p<0.001$, 5550 observations, 5538 d.f., 1 mouse, GLM F-
120 statistic=267, $p<0.001$. Finally, the mean $\Delta F/F$ ($\pm$CI, 4 mice) for the last second of odorant
121 application increases as a function of percent correct performance for the S+ condition
122 whereas it remains stable for the S- condition (Fig. 2g). A GLM analysis finds a statistically
123 significant difference between S+ and S- ($p<0.01$, 47 observations, 44 d.f., n=4 sessions, 4
124 mice, GLM F-statistic=60, $p<0.001$) and for the interaction between performance and the
125 odorant (S+ vs. S-) ($p<0.001$, 47 observations, 44 d.f., n=4 sessions, 4 mice
126 (Supplementary Fig. 6 shows learning curves for these mice). Therefore, as the animal
127 learns, the magnitude and temporal dynamics of the change in Ca^{2+} in MLIs diverges
128 between S+ and S- odorants, suggesting a possible role for MLIs in associative learning.
129 Interestingly, the majority of the ROIs responded similarly (Fig. 1c, Supplementary Fig. 4)
130 and a dimensionality analysis indicated that the dimensionality ranged from 2 to 6 (see
131 Supplementary Note 1 and Supplementary Fig. 7) indicating that the responses are highly
132 redundant.
133
134 **The identity of the stimulus can be decoded from MLI activity in proficient mice.** The
135 finding that the MLIs developed divergent responses for S+ vs. S- trials (Fig. 2g) raised
136 the question whether ensemble neural activity encodes for the identity of the stimulus. The
137 learning curve for a session where the mouse achieves >=80% in ~60 trials is shown in Fig.
138 3a. The first two principal components for a principal component analysis (PCA) of $\Delta F/F$
139 values for all MLIs in this session showed clear differences between S+ and S- trials for
140 the reward and odorant periods for trials when the mouse was proficient, in contrast to the

141 overlap observed between odorants for the naïve mouse (Fig. 3b). This suggested that
142 odorant identity (S+ vs. S-) could be decoded from ΔF/F values for proficient mice.
143
144 We utilized a linear discriminant analysis (LDA) to determine whether a hyperplane placed
145 in the multidimensional space of ΔF/F values for all MLIs in the ensemble could decode
146 the stimulus. The LDA was trained with ΔF/F for all trials minus one and was queried to
147 identify the odorant in the remaining trial (see Methods). The bootstrapped 95% confidence
148 interval (CI) for an LDA trained after shuffling stimulus was used as a control. The time
149 course for LDA decoding accuracy for the session with the learning curve in Fig. 3a is
150 shown in Fig. 3c (Supplementary Fig. 5a shows the corresponding lick frequency time
151 course). For trials with percent correct <=65%, decoding accuracy raises above the shuffled
152 95% CI after water reinforcement (Fig. 3ci), while for proficient trials, decoding accuracy
153 starts rising above CI shortly after odorant addition (Fig. 3cii). When tested in four mice
154 LDA decoding accuracy for the odorant and reinforcement periods differed from shuffled
155 LDA (Fig. 3d). A GLM analysis yielded statistically significant interactions between
156 shuffled vs. reinforcement and for the interactions between (shuffled vs. odorant) x
157 (proficient vs. naïve) and (shuffled vs. reinforcement) x (proficient vs. naïve) (GLM p
158 values <0.01 and <0.05, 24 observations, 18 d.f., n=4 sessions, 4 mice, GLM F-statistic
159 16.4, p<0.001). Post hoc tests corrected for multiple comparison using false discovery rate
160 (FDR)[33] yielded a statistically significant difference for decoding accuracy for either
161 reinforcement or odorant vs. shuffled for proficient (p<pFDR=0.007, n=4 sessions, 4
162 mice). Performing the analysis on subsets of ROIs showed that even analysis with a single
163 ROI yields decoding accuracy that is significantly different from the shuffled LDA

164 indicating that the information on the stimulus stored in MLI activity is highly redundant
165 (see Supplementary Note 2, Figs. 3e and f). The LDA analysis revealed that the accuracy
166 for decoding the odorant identity from ΔF/F during the odorant period increases as the
167 animal learns to differentiate between odorants.
168
169 **MLI odorant responses switch when stimulus valence is reversed.** In order to determine
170 whether the MLIs responded to the chemical identity of the odorant, as opposed to
171 responding to the valence (contextual identity: is the stimulus rewarded?), we reversed
172 odorant reinforcement. When the reward was reversed for a proficient mouse the animal
173 kept licking for the previous rewarded odorant resulting in a fall in percent correct below
174 50%, and as the animal learned the new valence the percent correct raised back above 80%
175 (Fig. 4a and Supplementary Figs. 6e and 6f). We analyzed how odorant-elicited changes
176 in MLI ΔF/F varied in this reversal task. Fig. 4b shows single trial examples for mean ΔF/F
177 odorant responses when the reward is reversed. MLIs respond to Iso (S+) with an increase
178 in ΔF/F before reversal (e.g. forward trial 52), maintain the odorant increase in ΔF/F to
179 what is now the unrewarded odorant (Iso, S-) immediately following reversal (reverse trial
180 92) and switch responses with increases to the new rewarded stimulus (MO, S+) when they
181 become proficient in the reversal task (reverse trial 438) (ΔF/F for the last second of the
182 odorant period is shown for all trials in Fig. 4c). When repeated for three different mice the
183 odorant-induced ΔF/F changes reversed for proficient mice (>=80% correct) when the
184 valence was reversed (Fig. 4d). GLM analysis indicates that there is a significant difference
185 in odorant-induced changes in ΔF/F for the odorant and the reversal ($p<0.001$, 12
186 observations, 8 d.f., n=3 sessions, 3 mice, GLM F-statistic=14.8, $p<0.01$). Thus, after

successful reversal the ΔF/F time course switched for the two odorants: the stimulus-induced increase in ΔF/F took place for the reinforced odorant, not for the chemical identity of the odorant.

Next we computed the accuracy for decoding the reinforced odorant for trials when the animal was proficient in either the forward or reverse trials using LDA analysis. Fig. 4e shows for the reversal session in Fig. 4a that for the proficient animal decoding accuracy rises above the 95% CI calculated with shuffled trials shortly after odorant addition for both forward and reverse trials. Finally, the results of the forward and reverse LDA analysis for three mice that are proficient showed that decoding accuracy for the stimuli differed from shuffled LDA (Fig. 4f). GLM analysis indicates that differences in decoding accuracy are statistically significant between original and shuffled ($P<0.001$), but not between forward and reverse ($p>0.05$, 12 observations, 8 d.f., n=3 sessions, 3 mice, GLM F-statistic=16, $p<0.001$). Finally, decoding accuracy of an LDA analysis for contextual identity for proficient mice did not differ between correct (Hits and CRs), and incorrect trials (Miss and FAs) (Supplementary Note 3, Supplementary Figs. 8,9). These results indicate that for the proficient mouse it is possible to decode contextual identity suggesting that MLI activity encodes for valence.

Changes in lick rate correlate with changes in MLI activity during reinforcement, but not during odorant application. To explore whether the observed MLI ensemble activity recorded in vermis is directly related to licking, as found in Crus II[34,35], we examined the correlation between ΔF/F and lick rate. When the animal was proficient the animal licked

210 at least once in each of the two lick segments during application of the S+ odorant,
211 increased licking after receiving the water reward and refrained from licking for the S-
212 trials (Fig. 5a). For the proficient mouse the lick frequency diverges between S+ and S-
213 trials shortly after addition of the odorant (Fig. 5b) and this divergence is evidenced by a
214 large decrease in the p value calculated with a ranksum test comparing licking between S+
215 and S- trials (Fig. 5c).
216
217 In order to explore the relationship of MLI activity to licking we proceeded to examine the
218 correlation between $\Delta F/F$ time course and the lick rate (LR) and between the derivative of
219 the $\Delta F/F$ time course ($D_t\Delta F/F$) and the derivative of the lick rate (D_tLR)[34] and plotted their
220 relationship during different time periods for proficient mice. Fig. 5d shows examples for
221 several trial outcomes for the time course for $\Delta F/F$ and the lick rate. Examples of these
222 correlations for a single session for a proficient mouse are shown in Figs. 5e and f. In this
223 example the correlation between $\Delta F/F$ and LR was larger during the reinforcement period
224 (ρ=0.73, p-value<0.001) compared to the odorant (ρ=0.19, p-value<0.001) and pre-odorant
225 (ρ=-0.06, p-value<0.05) periods (Fig. 5e). Similarly, the correlation between $D_t\Delta F/F$ and
226 D_tLR is significant for the reinforcement period (ρ=0.28, p<0.001), and is smaller for both
227 the pre-odorant (ρ=-0.08, p<0.05) and odorant (ρ=-0.045, p>0.05) periods (Fig. 5f). We
228 proceeded to compare the correlations between these parameters in several mice. As found
229 in Crus II, $\Delta F/F$ and LR (Fig. 5g) and $D_t\Delta F/F$ and D_tLR (Fig. 5h) are positively correlated
230 during the reinforcement period. Interestingly, the correlations are lower during the pre-
231 odorant and odorant periods (Figs. 5g,h). A t test indicated that there is a statistically
232 significant difference in the correlation coefficient between the reinforced vs. the odorant

233 or pre-odorant periods for ΔF/F vs. LR ($p<pFDR=0.05$, n=6 sessions, 5 mice) and between
234 the reinforced and odorant periods for D_tΔF/F vs. D_tLR ($p<pFDR=0.016$, n=6 sessions, 5
235 mice). These data suggest that changes in ΔF/F during the reinforcement period reflect
236 changes in lick activity, while changes in ΔF/F during the odorant period are less
237 dependent on licks, and maybe dependent on multiple variables. We performed
238 complementary studies of ΔF/F in CR trials when the mouse did not lick and for time-
239 courses aligned to the beginning of ΔF/F changes after odorant addition (Supplementary
240 Note 4 and Supplementary Figs. 10 and 11). Under these conditions, ΔF/F and lick rate are
241 uncorrelated, consistent with the potential lack of direct relationship between changes in
242 ΔF/F and lick rate during the odorant period.
243
244 **Do the MLIs respond to reward value?** The correlation between ΔF/F time course and
245 the lick rate (Fig. 5e) raises the question whether ΔF/F reflects the reward value as opposed
246 to the valence of the odorant. Here we define the valence of the odorant as indicating
247 whether the stimulus is good or bad[36]. Thus, valence is a binary measure of an emotion that
248 is reflected by the motivation to receive reward, whereas reward value, in the present
249 paradigm, is related to the amount of sugar water delivered. To evaluate whether ΔF/F
250 changes are dependent on reward value we recorded changes in ΔF/F from mice performing
251 a go-go task where both odorants were rewarded equally and we varied the volume of sugar
252 water delivered for successful trials. As expected, the mouse responded to both odorants
253 (Supplementary Fig. 12a). Also, as expected, when the volume of reward was increased,
254 the lick frequency increased during the delivery of sugar water (wet licks, Supplementary
255 Fig. 12b), but not during dry licking before reward (dry licks, Supplementary Fig. 12b). A

256 GLM analysis yielded a statistically significant difference for dry vs. wet licking and for
257 the interaction between the volume of sugar water delivered and dry vs. wet ($p<0.001$, 198
258 observations, 194 d.f., 1 session, 1 mouse, GLM F-statistic=21.8, $p<0.001$). In contrast, a
259 GLM analysis of the changes in $\Delta F/F$ as a function of volume delivered in dry and wet lick
260 conditions did not yield statistically significant changes (Supplementary Fig. 12c, $p>0.05$,
261 198 observations, 194 d.f., 1 session, 1 mouse, GLM F-statistic=1.7, $p>0.05$). Finally, if
262 MLI activity reflected reinforcement value $\Delta F/F$ should show a positive correlation with
263 volume of sugar water delivered (see Fig. 3 of [34]). We did not find a significant correlation
264 between lick frequency and $\Delta F/F$ for either dry (Supplementary Fig. 12di, $\rho=0.16$, $p>0.05$)
265 or wet licking (Supplementary Fig. 12dii, $\rho=-0.66$, $p>0.05$). This experiment indicates that
266 MLI activity does not reflect reward value, and is consistent with MLI activity reflecting
267 valence.
268
269 **The main contributor during odorant application to a GLM model fit to MLI activity**
270 **is the contextual identity of the odorant.** In order to understand the contribution of
271 different variables to MLI activity we setup a GLM to quantify the dependence of the
272 average $\Delta F/F$ on the different behavioral and stimulus variables[37]. We included "event"
273 variables, "whole trial" variables and "continuous" variables (Fig. 6a, Methods).
274 Continuous variables quantified kinematics including lick rate and the derivative of lick
275 rate (Fig. 5) and body velocity and body acceleration of movements made by the animal
276 during the trial (Supplementary Fig. 3). The identity of the odorant (S+/S- odorant) was an
277 event variable that increased from zero to one during the time for odorant application.
278 Finally, whole trial variables were accuracy (1 for correct and 0 for incorrect responses),

279 reinforcement history (1 for reinforcement in the last trial, 0 otherwise) and percent correct
280 behavior calculated in a window of 20 trials.
281
282 Black traces in Fig. 6b show examples of the fit of the GLM model to average ΔF/F time
283 courses for four example trials with different outcomes. The fit traces in black largely
284 overlap with the recorded data. When quantified over the different periods within a trial
285 (pre-odorant, odorant and reinforcement) we found that GLM explained a substantial
286 percent of the average ΔF/F variance ranging from 23.5% to 95% (Fig. 6c). We next
287 quantified the relative contribution of the different variables to the ensemble activity in the
288 three time periods. Fig. 6d shows the contributions to the GLM fit by the variables that
289 make the largest percent contribution to the fit (body kinematics, licks, reinforcement
290 history and odorants). Odorant (S+ vs. S-) is the dominant contributor to the activity during
291 odorant application (Fig. 6d,iii, asterisks show differences with ranksum or t test
292 $p<pFDR=0.033$, n=6 sessions, 5 mice). Furthermore, variables describing the licks
293 contribute to the GLM fit during the outcome period (Fig. 6d,ii, * $p<pFDR=0.016$ for a t
294 test, n=6 sessions, 5 mice). In contrast, the other two variables (body kinematics and
295 reinforcement history) do not differ in contribution during the different periods
296 ($p>pFDR=0.017$, ranksum test). These data indicate that odorant identity contributes to
297 modeling MLI activity during the odorant application period while licks contribute to MLI
298 activity during the reinforcement period.
299
300 **Chemogenetic inhibition of MLI activity leads to impaired go-no go learning.** In order
301 to determine whether activity of MLIs plays a role in behavioral responses in the go-no go

302 task we used a Cre-dependent AAV virus to express the inhibitory DREADDs receptor
303 hM4Di in MLIs in six PV-Cre mice (hM4Di group)[38]. To control for off-target effects of
304 clozapine-N-oxide (CNO)[39] we injected PV-Cre mice with Cre-dependent mCherry AAV
305 virus in another group of six mice (control group) (see Supplementary Fig. 13a,b for virus
306 expression). One to two weeks later animals from both groups were trained to differentiate
307 two odorant mixtures (S+: 0.1% of 60% heptanal+40% ethyl butyrate, S-: 0.1% of 40%
308 heptanal+60% ethyl butyrate) for 3-4 sessions encompassing 400-500 trials in the go-no
309 go task. The animals were injected intraperitoneally (IP) with saline 40 minutes before the
310 start of the sessions (control-saline and hM4Di-saline). One to two weeks later mice were
311 trained again to differentiate between the same odorant mixtures, but they were injected IP
312 with CNO (3mg/kg) 40 minutes before the start of the session (control-CNO and hM4Di-
313 CNO).
314
315 Figs. 7a,i and b,i show representative examples of the behavioral performance for the four
316 conditions. Mice in all groups with the exception of the hM4Di-CNO attained proficiency
317 (>=80% percent correct) (Figs. 7a,ii and 7b,ii). GLM analysis indicates that there is a
318 statistically significant interaction between CNO drug treatment and hM4Di expression
319 ($p<0.01$, 24 observations, 20 d.f., n=6 mice, GLM F-statistic=13.7, $p<0.001$) and post hoc
320 tests indicate that the hM4Di expressing group differs between CNO and saline
321 ($p<pFDR=0.025$, n=6 mice per group), while there are no significant differences between
322 CNO and saline for control mice ($p>pFDR$, n=6 mice per group), indicating an effect of
323 CNO-induced inhibition of MLIs expressing hM4Di on behavioral output and the absence
324 of off-target CNO effects.

We proceeded to compare the time course for lick frequency between different conditions for trials when the mouse was proficient (>=80% correct, Fig. 7c). Interestingly, the time course for lick frequency differs between hM4Di mice injected with CNO and the other conditions (Figs. 7c,i and 7c,ii). With the exception of hM4Di + CNO, shortly after odorant addition (~0.8 sec) the lick frequency for S- does not increase beyond ~1 Hz while the lick frequency for S+ keeps increasing beyond 8 Hz (Fig. 7c). In contrast, for hM4Di + CNO lick frequency for S- keeps increasing beyond 1 Hz and does not diverge from the S+ time course until it reaches 2.5 Hz at a later time point (~1 sec, Fig. 7c,ii) likely reflecting slow decision-making. This would explain why the hM4Di + CNO mice accumulated errors in the go-no go task (Fig. 7bii). In order to quantify this difference in lick frequency we calculated the lick frequency 0.8 to 1.8 seconds after odorant addition (Fig. 7d). For S+ GLM analysis did not find a statistically significant difference for treatment or hM4Di expression (or interactions) for the rewarded odorant trials (Fig. 7di, $p>0.05$, 60 observations, 56 d.f., n=6 mice, GLM F-statistic=2.96, $p>0.05$). Yet GLM found a statistically significant difference for S- for the interaction between CNO and hM4Di expression (Fig. 7dii, $p<0.001$, 60 observations, 56 d.f., n=6 mice, GLM F-statistic=12.8, $p<0.001$). We obtained a similar impairment of performance in a separate set of experiments with two hM4Di mice and two controls where animals discriminated between 1% Iso and MO, and CNO was applied when the animal was naïve, and we reversed the reward (Supplementary Fig. 13). These data indicate that inhibition of MLIs causes a slower differential lick response to odorants leading to impaired behavioral performance.

347 **Discussion**

348

349 We found that vermal MLIs developed a differential response to odorants in the go-no go
350 task that switched when the valence was reversed. Decoding analysis revealed that when
351 the animal was proficient the contextual identity of the odorant could be decoded from MLI
352 responses. GLM analysis revealed that contextual identity made a large contribution to the
353 fit of MLI activity during the odorant application period. Chemogenetic inhibition of MLIs
354 impaired achievement of proficient discrimination of odorants. These data indicate that
355 MLIs play a role in associative learning by encoding valence.

356

357 The cerebellum has been implicated in mediating supervised learning through an iterative
358 process whereby the response to an input is evaluated against a desired outcome, and errors
359 are used to adjust adaptive elements within the system[8-10,40]. CFs carrying error signals
360 make profuse synaptic connections on the dendrites of PCs and elicit powerful excitatory
361 dendritic Ca^{2+} spikelets[41-44]. Furthermore, CFs also signal reward prediction[11,12] or
362 decision-making errors[13], and the cerebellum modulates association pathways in VTA
363 enabling a cerebellar contribution to reward-based learning and social behavior[14]. The
364 increase in Ca^{2+} mediates LTD in subsets of synapses innervated by co-activated GC
365 parallel fibers (PFs) carrying sensorimotor information relevant to learning[45,46]. However,
366 recent studies by Rowan et al.[25] revealed that increasing feed forward inhibition by MLIs
367 can switch the valence of plasticity from LTD to LTP (also, see[47]). In addition, adaptive
368 changes in the vestibulo-ocular reflex elicited by CF optogenetic activation switched from
369 increase to decrease depending on whether MLIs were co-activated[25]. Finally, MLIs gate

370 supralinear CF-evoked Ca2+ signaling in the PC dendrite[48]. These studies suggest that the
371 valence of learning is graded by MLI activity.
372
373 Here we provide evidence for the involvement of MLIs in conveying information on
374 contextual identity of a stimulus in associative learning. We do not find that the MLIs
375 respond to odorants per se. Rather, the reversal experiment (Fig. 4) and the similar ΔF/F
376 responses and stimulus decoding for correct and incorrect behavioral response trials
377 (Supplementary Fig. 8) indicate that MLIs respond to contextual odorant identity: "is this
378 the rewarded odorant?", which is directly related to valence, a binary measure of an
379 emotion reflected by the motivation to receive reward[36]. Furthermore, our results in the go-
380 go task where both odorants are rewarded with varying volumes of sugar water
381 (Supplementary Fig. 12) are consistent with the response reflecting valence (as opposed to
382 value). Thus, we postulate that the MLI response during the odorant period is related to
383 valence that reflects reward expectation, consistent with the fact that GCs in lobe VI were
384 found to respond to reward expectation[29,30].
385
386 A question that arises is which circuit mechanism is responsible for the decreased
387 behavioral performance after chemogenetic inhibition of MLI activity (Fig. 7 and
388 Supplementary Fig. 13). MLIs receive sensorimotor information from multiple GCs
389 through PF input and *in vivo* studies have found remodeling of MLI receptive fields upon
390 repeated electrical stimulation of the skin[49]. In addition, plasticity in PF-MLI synapses are
391 postulated to increase the information capacity of the MLI-PC network and richness of PC
392 output dynamics[10,16], and a model of PF-MLI plasticity has been proposed[50]. If long term

393 plasticity of PF-MLI synapses is responsible for the large change of MLI responsiveness
394 found here upon reversal of stimulus valence it is likely that the error signal would be
395 provided by CF spillover resulting in highly redundant stimulation of stellate cells
396 (SCs)[51,52]. We developed a model of the MLI/PC circuit described in Supplementary Note
397 5 (Supplementary Figs. 14,15) that suggests that plasticity in SC-PC synapses[53], PF-SC
398 synapses[50], complemented with CF spillover acting on the feedforward disinhibitory MLI
399 circuit described recently by Arlt and Hausser[52], complemented with plasticity in SC-PC
400 synapses[53], PF-SC synapses[50], would explain the changes in behavior we find after
401 chemogenetic inhibition of MLI activity. Finally, we found that the divergence between
402 the time courses for lick frequency between S+ and S- took place at a later time when MLIs
403 were inhibited by chemogenetics (Fig. 7c,ii, Supplementary Fig. 13g) likely reflecting slow
404 decision-making, consistent with a role for the CF/PC circuit in reward timing prediction[54].
405 Future studies are necessary to understand the role of plasticity in the PF-MLI-PC circuit
406 in associative learning.
407

408 Interestingly, odorant responses have been reported in the cerebellum. Studies in sexually
409 trained male rats found that female bedding or almond smell elicited increased cFos
410 immunoreactive GCs in the vermis compared to rats exposed to clean air[55]. Furthermore,
411 sexual experience increased the number of cFos positive GCs. In humans odorants induced
412 significant activation of the cerebellum[56]. In addition, human cerebellar lesions caused
413 olfactory impairments in the contralesional nostril, and elicited sniffs with lower overall
414 airflow velocity compared to controls[57]. These findings implicate an olfactocerebellar
415 pathway prominent in odorant identification and detection that functionally connects each

416 nostril primarily to the contralateral cerebellum. Our study provides further evidence for
417 involvement of the cerebellum in olfactory tasks.
418
419 Here we found changes in MLI activity during learning in the go-no go associative learning
420 task in lobule VI where GCs[29,30] and CF[58] activity was proposed to encode aspects of
421 reward signaling. Recent work on the contribution of cerebellar processing to execution of
422 reward-driven behaviors indicates that multiple cerebellar regions are involved, including
423 central and lateral cerebellum[11,29,30,58,59]. As behavioral tests are refined, it is likely that
424 differences in how these regions process reward will emerge, as suggested by the recent
425 work on climbing-fiber signaling[11]. Furthermore, we focused our recordings on the more
426 superficial regions of the molecular layer and therefore, most of our measurements are from
427 SCs. Recordings from synaptically connected pairs of MLIs and PCs in slices showed that
428 mean the amplitude of synaptic currents decreases with distance from the PC layer,
429 suggesting a stronger impact of basket versus SC inhibition on PC firing[60]. Recent
430 recordings of PC spikes in vivo following genetic deletion of MLIs confirm this
431 prediction[47] which is in accord with the morphological diversity of MLIs[61]. Finally, the
432 effect of chemogenetics (Fig. 7) should be on both stellate and basket cells, and future
433 experiments are necessary to differentiate between the roles of the two cell types.
434
435 Our findings show that differential MLI activity develops during learning in an associative
436 learning task and that MLI activity switches when the rewarded odorant is reversed. We
437 find that inhibition of MLI activity elicits decreased behavioral performance in the go-no
438 go task. Our data indicate that MLIs have a role in learning valence. This would likely

increase the information capacity of the MLI-PC network and richness of PC output dynamics[10,62].

Acknowledgments: We thank Ms. Nicole Arevalo for animal husbandry, Ms. Dnate' Baxter for laboratory support, Ms. Arianna Gentile-Polese for help with the summary figure and Mr. Jesse Gilmer with help coding dimensionality. We thank Mr. Matt I. Becker, Mr. Jesse Gilmer and Dr. Abigail Person for discussions. This research was supported by NIDCD R01 DC000566, NINDS U01 NS099577, NSF CBET-1631912, NSF BIO-1926676 and ANR-18-CE16-0010-01.

.

Author contributions: M.M., I.Ll. and D.R. designed all experiments aided with discussions with E.G., B.O., F.S. and G.F., while M.M. G.F. and D.R. performed them. E.G., G.F. and B.O. designed, setup and maintained the custom two-photon microscope, M.M. and D.R. set up the olfactometer. D.R. wrote all programs for data collection and analysis. F.S. performed circuit modeling, M.M. and D.R. analyzed the data. M.M. and D.R. generated the figures. All authors discussed the results. M.M. and D.R. wrote the manuscript, and all authors participated in commentary and revision of the manuscript.

Declaration of interests: The authors declare no competing interests.

462 **Methods**

463 **Animals**

464 All animal procedures were performed in accordance with protocols approved by the
465 Institutional Animal Care and Use Committee of the University of Colorado Anschutz
466 Medical Campus. Mice were bred in the animal facility. We used both male and female
467 adult Parvalbumin-Cre (PV-Cre, Stock number 008069, Jackson Laboratory, USA) mice
468 and wild-type C57BL/6J mice. The animals were housed in a vivarium with a 14/10h
469 light/dark cycle. Food was available ad libitum. Access to water was restricted in for the
470 behavioral training sessions according to approved protocols, all mice were weighed daily
471 and received sufficient water during behavioral training to maintain >=80% of original
472 body weight.

473

474 **Immunohistochemistry**

475 To perform immunostaining, mice were sacrificed and transcardially perfused with ice cold
476 4% paraformaldehyde (Electron Microscopy Sciences, USA), followed by incubation in
477 30% sucrose (Sigma-Aldrich, USA). After the brain was incubated in the sucrose solution
478 60 μm thick slices were cut with a cryostat. The slices were imaged using a confocal laser
479 scanning microscope (Leica TCS SP5II, Germany or Nikon A1R, Japan) to determine the
480 GCaMP expression patterns in the cerebellum. The slices were counterstained with DAPI
481 (Thermo Fisher Scientific, USA).

482

483 **Window implantation**

484 Adult mice (8 weeks or older) were first exposed to isoflurane (2.5%) and then maintained
485 anesthetized by intraperitoneal ketamine-xylazine injection (100 μg/g and 20 μg/g). A
486 craniotomy was made over the vermis of cerebellum centered at midline 6.8 mm posterior
487 to Bregma leaving the dura intact (lobule VI). A square glass window (2 mm x 2 mm) of
488 No 1 cover glass (0.13 to 0.17 mm thick, Thermo Fisher Scientific, USA) was placed over
489 the craniotomy and the edges were sealed with cyanoacrylate glue (3M, USA). The window
490 was further secured with Metabond (Parkell, USA), and a custom-made steel head bracket
491 was glued to the skull.
492
493 **Virus expression of GCaMP**
494 In order to express GCaMP6f in cerebellar MLIs we injected the vermis of the cerebellum
495 in three adult PV-Cre mice with 2.0 μl of AAV1-Syn-Flex-GCaMP6f (Addgene, USA)
496 (6.8 mm posterior to Bregma, bilaterally ±0.5 mm lateral to midline and 200-400 μm below
497 the brain surface)[63]. The viral infection method we use has been reported to express
498 GCaMP in MLIs, and not in PCs[64,65]. Supplementary Fig. 2 shows that indeed expression
499 of GCaMP6 takes place only in MLIs. Note the absence of fluorescence from GCs as well
500 as from PC somata and dendrites. Expression in MLIs may reflect the differential activity
501 of the hSyn promoter, and has been described for a different genetically-encoded Ca^{2+}
502 indicator[65]. In one C57BL/6 animal each we used AAV5-Syn-GCaMP6s or AAVrg-Syn-
503 jGCaMP7f (Addgene, USA) with similar results to those obtained with GCaMP6f
504 (Supplementary Fig. 16a) and therefore the data were pooled. After the injection, the
505 animals were maintained for at least three weeks before behavior training and imaging.
506

507 **Go-No Go training**

508 Mice were water deprived by restricting daily consumption of water to 1-1.5 ml. Mice were
509 monitored for signs of dehydration or a decrease in body weight below 80% of the initial
510 weight. If either condition occurred the animals received water ad-lib until they recovered.
511 When the animals were thirsty, they were trained in a head-fixed olfactory go-no go task
512 with (1% Iso vs MO odorant application, Sigma-Aldrich, USA)[26,66]. Licks were monitored
513 by an electrical circuit monitoring the resistance between the lick spout and the floor in an
514 olfactometer that controlled valves to deliver a 1:40 dilution of odorant at a rate of 2 lt/min.
515 The water-deprived mice started the trial by licking on the water port. The odorant was
516 delivered after a random time interval ranging from 1 to 1.5 seconds. In S+ trials, the mice
517 needed to lick at least once in two 2 sec lick segments to obtain a reward (0.1 g/ml sucrose
518 water) (Fig. 1a). The inter trial interval (ITI) was 22.3-22.8 sec. In S- trials, the mice need
519 to refrain licking one of the two 2 sec segments to avoid a longer inter-trial interval (22.3-
520 22.8 + 10 sec). The animal's behavior performance was evaluated in a sliding window of
521 20 trials and the calculated value was assigned to the last trial in the window. Therefore, it
522 estimates the performance in the last 20 trials. The percent correct value represents the
523 percent of trials in which the animal successfully performed appropriate actions, and we
524 considered the animal proficient if percent correct performance is above 80%. In reverse
525 go-no go training sessions, the rewarded and un-rewarded odorants were switched.
526 Movement of the mouse was imaged in the infrared to prevent light interference with the
527 non-descanned detection in the visible using a 1 Megapixel NIR security camera (ELP-
528 USB100W05MT-DL36, Amazon.com, USA) at 30 frames per second. Velocity of body
529 movement was estimated using the Farneback algorithm coded in Matlab[67] (Mathworks,

530 USA). Measurement of body movement with a single camera gives limited information.
531 Five mice were used for the go-no go experiments. Four mice were imaged when they were
532 naïve. The window became opaque for two of the mice preventing MLI imaging for the
533 reversal experiment.
534
535 **Go-Go training**
536 For the experiment in Supplementary Figure 12 both odorants were rewarded with the same
537 volume of sugar water, and the volume of sugar water reward was varied. The two odorants
538 in this experiment were either 1% Iso and MO, or the same odorant 1% Iso and 1% Iso.
539 The results were similar for both odorant pairs, and the analysis was performed for all trials
540 regardless of odorant pair.
541
542 **Behavioral performance recorded after chemogenetic inhibition of MLI activity**
543 For chemogenetic inhibition of MLI activity[38,39], 1.2 ul of AAV8-hSyn-DIO-hM4D(Gi)-
544 mCherry virus (Addgene, USA) were bilaterally injected into 6 PV-Cre animals bilaterally
545 ±0.5 mm lateral to midline, 6.8 mm posterior to Bregma and 200-400 μm below the brain
546 surface. For control an AAV8-hSyn-DIO-mCherry virus (Addgene, USA) was injected in
547 the same position in 6 PV-Cre animals. This viral infection method results in expression of
548 the protein in MLIs, and not in PCs[64,65]. We performed two separate experiments: 1) For
549 the experiments in Fig. 7 four weeks after injection the animals were trained to proficiency
550 in the go-no go task with 1% Iso (S+) vs MO (S-). When they reached a proficient level,
551 the animals rested for one to two weeks, and were then injected intraperitoneally (IP) with
552 saline 40 minutes before starting the session and were trained to discriminate between two

553 odorant mixtures: 0.1% of 60% heptanal+40% ethyl butyrate (S+) (Sigma-Aldrich, USA)
554 and 0.1% of 40% heptanal+60% ethyl butyrate (S-) for 3-4 sessions for a total of 400-500
555 trials. The animals then rested for one to two weeks and were subsequently trained to
556 discriminate the same odorant mixtures in sessions that took place 40 minutes after IP
557 injection of 3mg/kg clozapine-N-oxide (CNO, Tocris, USA). 2) For the experiment in
558 Supplementary Fig. 13 the animals were naïve for the discrimination of Iso vs. MO. The
559 animals were injected intraperitoneally (IP) with 3mg/kg clozapine-N-oxide (CNO, Tocris,
560 USA) 40 minutes before starting the session and were trained to discriminate between 1%
561 Iso (S+) and MO (S-) for 6 sessions for a total of 500-600 trials. The reinforcement was
562 then reversed and the animals were again injected with CNO 40 minutes before the sessions
563 and were trained to discriminate between MO (S+) and 1% Iso (S-) for 5 sessions for a
564 total of 400-500 trials.
565
566 **Two photon imaging of MLI activity in animals undergoing the Go-No Go task**
567 All the animals were first habituated to the setup to minimize stress during the imaging
568 experiments. All the imaging sessions started at least 10 minutes after mice had been head-
569 fixed. We searched for active MLIs while imaging zones in the vermis of lobule VI,
570 between the midline and the paravermal vein, an area of the cerebellum where GCs acquire
571 a predictive feedback signal or expectation reward[29,30]. The head fixed two photon imaging
572 system consisted of a movable objective microscope (MOM, Sutter Instrument Company,
573 USA) paired with a 80 MHz, ~100 femtosecond laser (Mai-Tai HP DeepSee, Spectra
574 Physics, USA) centered at 920 nm. The MOM was fitted with a single photon
575 epifluorescence eGFP filter path (475 nm excitation/500-550 nm emission) used for initial

576 field targeting followed by switching to the two photon laser scanning path for imaging
577 GCaMP at the depth of the MLIs. The galvometric laser scanning system was driven by
578 SlideBook 6.0 (Intelligent Imaging Innovations, USA). The two photon time lapses were
579 acquired at 256 x 256 pixels using a 1.0 NA/20x water emersion objective (Zeiss,
580 Germany) at 5.3 Hz. On the day of initial imaging, a FOV was selected to image a large
581 number of active cerebellar neurons located in the most superficial planes of the molecular
582 layer (within 50 μm beyond the dorsal surface of the molecular layer) including mostly
583 SCs, and several batches of 6000 frames ("time series") were collected in each training
584 session. After two photon imaging a second image of the vasculature was captured with
585 wide field epifluorescence to reconfirm the field.
586
587 **Data analysis**
588 Raw imaging data was first surveyed in ImageJ (NIH, USA) to exclude image sequences
589 exhibiting axial movement. We did not find evidence of axial movement while the animal
590 was engaged in the go-no go task. In addition, we performed control imaging where we
591 excited GCaMP6f at 820 nm, a two photon excitation wavelength where fluorescence
592 emission is Ca^{2+}-independent[68]. Supplementary Fig. 16b,c shows that we did not detect
593 transient changes in GCaMP6 fluorescence in a mouse engaged in the go-no go task when
594 the cells were excited at 820 nm. If we found horizontal drift due to motion, we applied
595 cross correlation-based image alignment using the Turboreg, Image J plugin. The data were
596 then analyzed with CaImAn Matlab software that uses constrained nonnegative matrix
597 factorization to define independent spatial and temporal components corresponding to
598 changes in GCaMP fluorescence in individual MLIs[31]. Baseline of intensity ($F0$) was

599 defined as the mean fluorescence intensity before trial start, defined as the time when
600 the animal first licked. This was when fluorescence started to increase above baseline
601 and the odorant was added at a random time 1-1.5 seconds after trial start. Intensity
602 traces (F) were normalized according to the formula $\Delta F/F = (F - F0)/F0$. After CaImAn
603 analysis, the ΔF/F traces of the spatial components were sorted and we assigned trial traces
604 to different behavioral events (Hit, CR, Miss and CR) and aligned them to trial start,
605 odorant onset or water delivery. Finally, the time course for the average ΔF/F did not differ
606 greatly between the different GCaMP variants as would be expected for a fast firing
607 interneuron with small increases in Ca^{2+} per action potential (Supplementary Fig. 16a).
608
609 **Statistical analysis**
610 Statistical analysis was performed in Matlab (Mathworks, USA). Statistical significance
611 for changes in measured parameters for factors such as learning and odorant identity (S+
612 vs. S-) was estimated using a generalized linear model (GLM), with post-hoc tests for all
613 data pairs corrected for multiple comparisons using false discovery rate[33]. The post hoc
614 comparisons between pairs of data were performed either with a t-test, or a ranksum test,
615 depending on the result of an Anderson-Darling test of normality. 95% CIs shown in the
616 figures as vertical black lines or shading bounding the lines were estimated by bootstrap
617 analysis of the mean by sampling with replacement 1000 times using the bootci function
618 in MATLAB.
619
620 Principal component analysis was calculated using the Matlab Statistics Toolbox.
621 Classification of trials using ΔF/F measured from all components in the FOV was

622 accomplished via linear discriminant analysis (LDA) in Matlab. We obtained similar result
623 with perceptron analysis (not shown). ΔF/F for all components for every trial except one
624 were used to train the LDA, and the missing trial was classified by its fit into the pre-
625 existing dataset. This was repeated for all trials and was performed separately for analysis
626 where the identity of the odorants was shuffled. Fluorescence intensity traces, lick rates
627 and kinematics in Fig. 6 were low-pass filtered with a hamming window of a time
628 constant of 0.59 s.

629

630 **Dimensionality**

631 Following Litwin-Kumar et al.[69] we defined the dimension of the system (dim) with *M*
632 inputs as the square of the sum of the eigenvalues of the covariance matrix of the measured
633 ΔF/F for all ROIs in the FOV divided by the sum of each eigenvalue squared:

634 $$\dim(\Delta F/F) = \left(\sum_{i=1}^{M} \lambda_i\right)^2 / \left(\sum_{i=1}^{M} {\lambda_i}^2\right)$$

635

636 where λ_i are the eigenvalues of the covariance matrix of ΔF/F computed over the
637 distribution of ΔF/F signals measured in the FOV. If the components of ΔF/F are
638 independent and have the same variance, all the eigenvalues are equal and dim(ΔF/F) = *M*.
639 Conversely, if the ΔF/F components are correlated so that the data points are distributed
640 equally in each dimension of an *m*-dimensional subspace of the full *M*-dimensional space,
641 only *m* eigenvalues will be nonzero and dim(ΔF/F) = *m*.

642

643 **Generalized linear modelling estimate of contribution of different variables to**
644 **changes in ΔF/F**

645 In order to quantify the contribution of different variables to neural activity, we used GLM
646 as described by Engelhard et al. [37]. We used the Matlab fitglm function to fit the per trial
647 ΔF/F time course for mice proficient in the go-no go task with a GLM. We included "event"
648 variables, "whole trial" variables and "continuous" variables. Continuous variables
649 quantified kinematics including lick rate, the derivative of lick rate and the velocity and
650 acceleration of movements made by base of the tail of the head fixed animal during the
651 trial (body velocity and body acceleration, see Supplementary Fig. 3). The identity of the
652 odorant (S+/S- odorant) was an event variable that increased from zero to one during the
653 time for S+ or S- odorant application. Finally, whole trial variables were accuracy (1 for
654 correct responses and 0 for incorrect responses), reinforcement history (1 for reinforcement
655 in the last trial, 0 otherwise) and percent correct behavior calculated in a window of 20
656 trials.

657

658

659

660 **Data availability**

661 The data supporting the findings of this study are available in GigaDB (http://gigadb.org/)
662 (we are depositing the data in GigaDB, and this line will be replaced with a link to the data),
663 the model is deposited in ModelDB (https://senselab.med.yale.edu/modeldb/)(we are
664 depositing the data in ModelDB, and this line will be replaced with a link to the data) and
665 the code is available in https://github.com/restrepd/CaImAnDR.

666 **Table 1. Percent of ROIs displaying a change in ΔF/F during odorant application**

667

Calculation	Percent responsive	Number	Number of ROIs
Percent of ROIs responding in Hit trials	99.9±0.23	21 time series, 5 mice	74-199
Percent of ROIs responding in CR trials	82.3±26	21 time series, 5 mice	74-199
Percent of ROIs responding in Miss trials	97.8±6.5	13 time series, 5 mice	105-199
Percent of ROIs responding in FA trials	78±29	15 time series, 5 mice	74-199
Percent of ROIs responding in Miss trials that also respond in Hit trials	99.96±0.15	13 time series, 5 mice	105-199
Percent of ROIs responding in FA trials that also respond in Hit trials	99.8±0.47	15 time series, 5 mice	74-199

668

669 This calculation was performed in time series that included at least one Miss or FA trial

670 when the animal was proficient (percent correct >=80%). The ROI was classified as

671 responsive when ΔF/F increased above or decreased below baseline ΔF/F by 2.5 x SD.

672 Baseline mean and SD were calculated for the time interval 10 to 2 sec before odorant

673 onset.

674

675

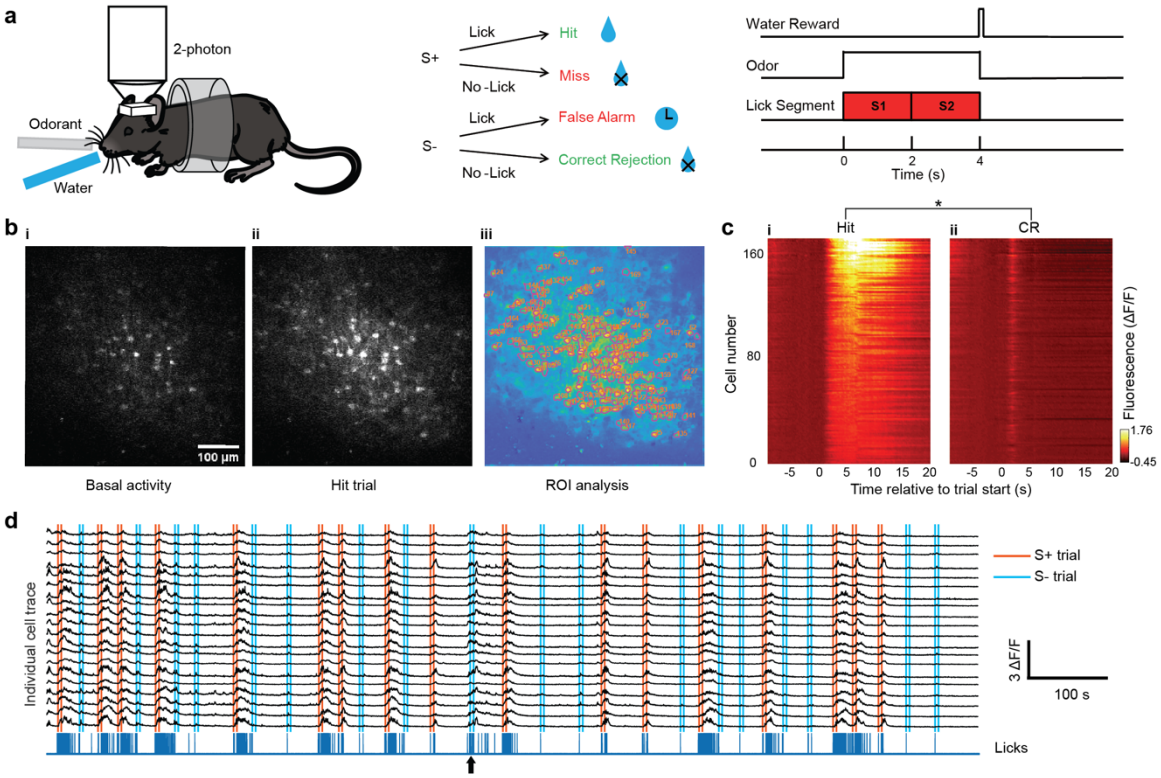

Figure 1. Two-photon Ca^{2+} imaging of MLIs in head-fixed mice undergoing the go-no go associative learning task.

a. Go-no go task. Left: Two-photon imaging of a head-fixed mouse responding to odorants by licking on a water spout in response to the rewarded odorant in the go-no go task. Center: Scoring of decision making. Right: time course of the trial. For water reward in Hit trials the animal must lick at least once in each of the two 2 second lick segments.

b. The panels in **i** and **ii** show two photon microscopy images of GCaMP6f fluorescence recorded from MLIs in a mouse proficient in the go-no go task (basal activity: before trial start, Hit trial: during reinforced odorant application). The color image in **iii** shows the regions of interest identified using CaImAn software[31].

c. Pseudocolor plots displaying the average per trial ΔF/F time course for Hit (**i**) and CR (**ii**) odorants for all ROIs in this example. GLM analysis involving time periods pre-odorant

(1 sec before odorant onset), odorant (last second during odorant application) and reinforcement (1.5 second after reinforcement) and different events (Hits, Miss, CR and FA) yielded significant differences between reinforcement and pre-odorant ($p<0.001$), between odorant and pre-odorant ($p<0.001$), and between all interactions between these two period pairs and all events ($p<0.01$, 2040 observations, 2028 degrees of freedom, n=170 ROIs, 1 mouse, GLM F-statistic 234, $p<0.001$). *Post-hoc ranksum $p<pFDR=0.048$. **d**. Neural ensemble activity. Black traces are the GCaMP6f fluorescence ($\Delta F/F$) time courses for a subset of the ROIs identified in the FOV in **b**. This mouse was proficient (>=80% correct trials). Vertical lines: orange start and end of S+ odorant application, light blue is S-. The blue trace at the bottom shows the licks. All trials were Hits or CRs with the exception of the trial identified with the arrow that was a FA. Data shown in panels b-d are from one session (one mouse).

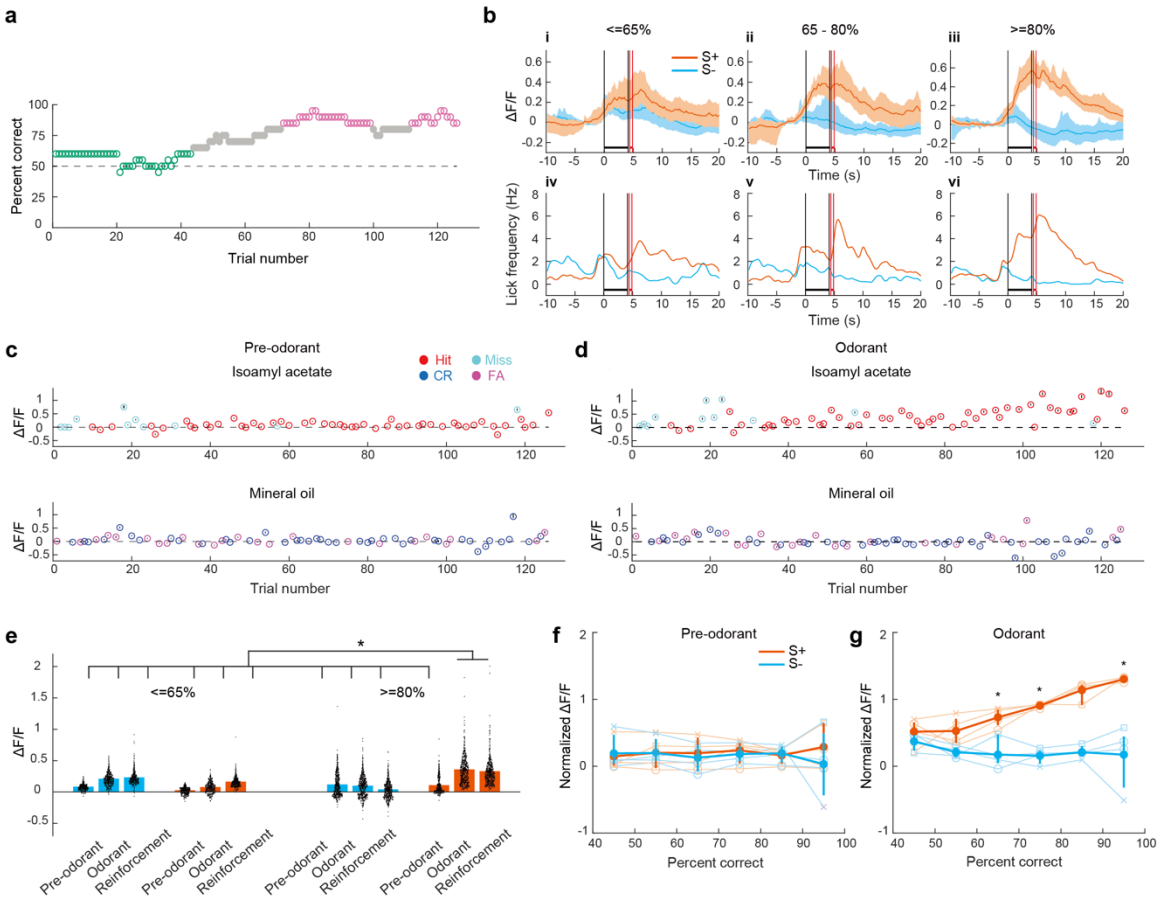

Figure 2. MLIs developed divergent responses during go-no go learning.

a. Learning curve for a mouse discriminating 1% Iso from MO in the go-no go task. Magenta dots: proficient level (>=80% percent correct), green dots: naïve level (percent correct <=65%).

b. GCaMP6f fluorescence (ΔF/F) time course averaged over all ROIs and trials falling within different proficiency windows shown for the session whose performance is shown in **a**. **i.** <= 65% (naïve), **ii.** 65%-80% and **iii.** >= 80% (proficient). Orange: S+, light blue: S- (the shaded area is the 95% CIs). The vertical black lines are odorant onset and removal and the red lines bound the reinforcement period.

714 **c-d**. Per trial ΔF/F averaged over all ROIs for one second before odorant application (**c**,
715 Pre-odorant**)** and in the last second during odorant application (**d,** Odorant) shown for the
716 session in **a**. Vertical lines around the mean of each trial are the CI.
717 **e.** Violin plot showing per ROI ΔF/Fs for the session shown in **a** for the following time
718 windows: pre-odorant (one second before odorant application), odorant (the last second of
719 odorant application) and reinforcement (one and a half seconds after onset of
720 reinforcement). Per ROI ΔF/Fs are shown for trials falling within different proficiency
721 windows: <= 65% (naïve) and >= 80% (proficient). A GLM indicates that there are
722 significant differences between S+ (orange) and S- (light blue), between time windows and
723 between naïve and proficient mice ($p<0.001$, 5538 d.f., one mouse, *post-hoc ranksum/t
724 test p value < pFDR=0.043).
725 **f-g**. ΔF/F for four mice averaged over all the ROIs for all trials falling within different
726 proficiency windows. ΔF/F average was calculated for one second before odorant
727 application (**f**) and for the last second during odorant application (**g**). For the data during
728 odorant application (**g**) a generalized linear model (GLM) analysis indicated that there is a
729 statistical significance for the interaction between percent correct and the identity of the
730 odorant ($p<0.001$, 43 d.f., n=4 sessions, 4 mice, GLM F-statistic=60, $p<0.001$). GLM did
731 not yield statistically significant differences for pre-odorant data (**f**, $p>0.05$, 43 d.f., n=4
732 sessions, 4 mice, GLM F-statistic=0.46, $p>0.05$)**.** *Post-hoc t-test, p<pFDR=0.018.
733
734
735

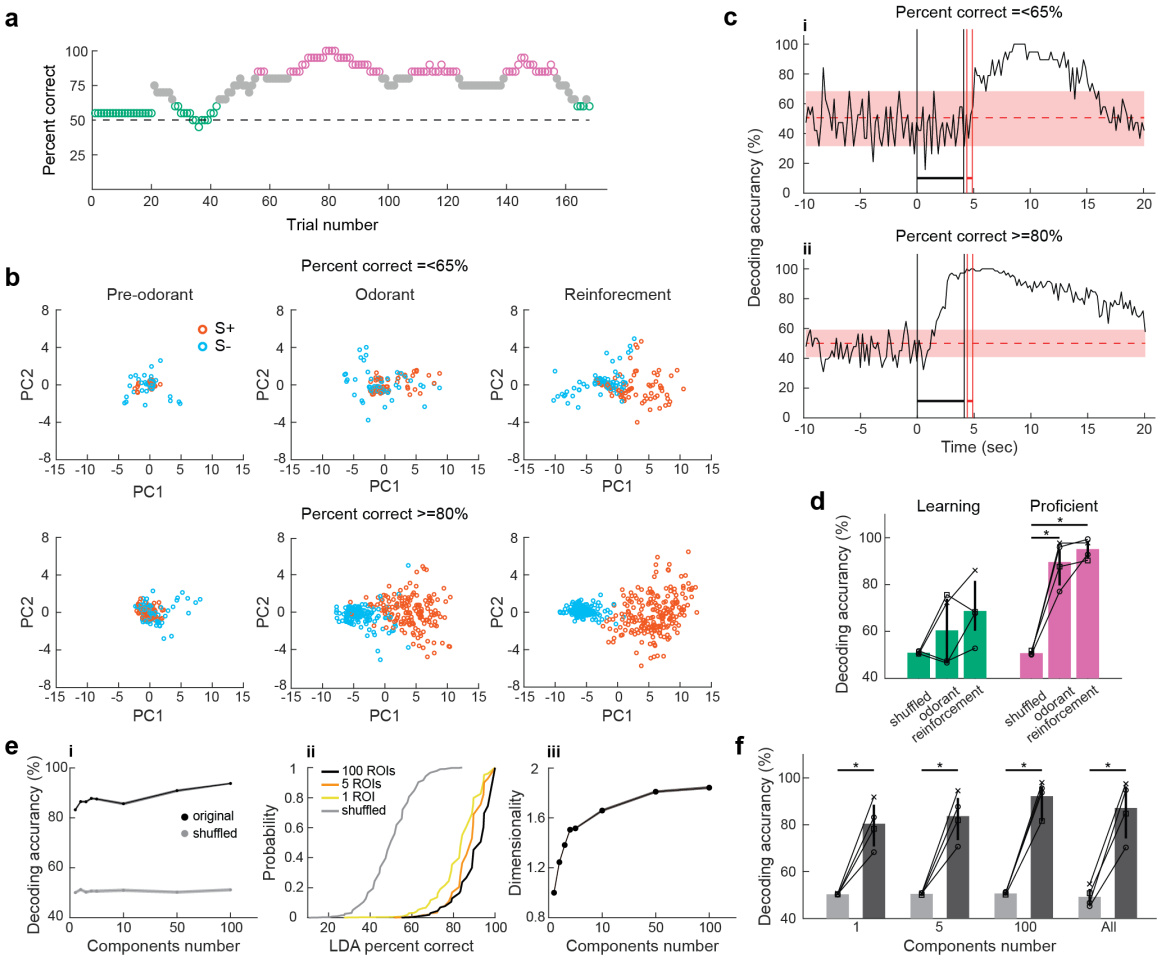

Figure 3. The accuracy of decoding the stimulus increases as the animal learns to discriminate the odorants.

Panels **a-c** show behavioral performance (**a**), PCA analysis (**b**) and LDA analysis (**c**) for one session (one mouse). **a**. Learning curve for a mouse performing the head-fixed go-no go task. Magenta dots: proficient level (>=80% percent correct), green dots: percent correct <=65%.

b. First two principal components for the PCA for the changes in GCaMP6f fluorescence (ΔF/F) in all the ROIs in the FOV. Top: the mouse was performing =< 65% correct, bottom: the same mouse was performing >=80% correct. The principal components are shown for three time periods: Pre-odorant: 1 sec before odorant addition, odorant: 1 sec before

747 removal of the odorant, and Reinforcement: 1.5 sec after reward. Orange circles: S+ trials,
748 light blue circles: S- trials.
749 **c**. Decoding accuracy for the linear discriminant analysis (LDA) trained to predict odorant
750 identity using ΔF/F for all ROIs in the FOV. Shade: 95% CI for LDA trained with shuffled
751 odorant identity. The vertical black lines are odorant onset and removal and the red lines
752 bound the reinforcement period.
753 **d**. LDA decoding accuracy calculated from the (ΔF/F) for all ROIs in the FOV from data
754 recoded in four mice. A GLM analysis of decoding accuracy yielded statistically significant
755 interactions between (shuffled vs. odor) x (proficient vs. naïve) and for (shuffled vs.
756 reinforcement) x (proficient vs. naïve) (GLM p values <0.01 and <0.05, 24 observations,
757 18 d.f., n=4 sessions, 4 mice, GLM F-statistic=16.4, p<0.001). The vertical lines show 95%
758 CIs. *Post hoc t-tests corrected for multiple comparison using false discovery rate (FDR,
759 p<pFDR=0.007, n=4 sessions, 4 mice).
760 **e.** Example of LDA decoding analysis performed with subsets of ROIs ranging from 100
761 to 1 ROI. The analysis was performed for one session for trials where the mouse was
762 proficient (percent correct >=80%). **i.** Decoding accuracy (mean± 95% CI) as a function of
763 the number of ROIs. **ii.** Cumulative probability histograms for the decoding accuracy for
764 the different number of ROIs and for the shuffled LDA. **iii.** Dimensionality as a function
765 of the number of ROIs.
766 **f.** Summary graph showing the decoding accuracy for different numbers of ROIs (mean±
767 95% CI, 4 sessions, 4 mice). A GLM analysis indicated that the decoding accuracy for the
768 shuffled analysis was statistically different from accuracy with the subsets of ROIs

769 ($p<0.001$, 72 observations, 54 d.f., n=4 sessions, 4 mice, GLM F-statistic=23.6, $p<0.001$).

770 *Post-hoc t-tests or ranksum $p<pFDR=0.03$.

771

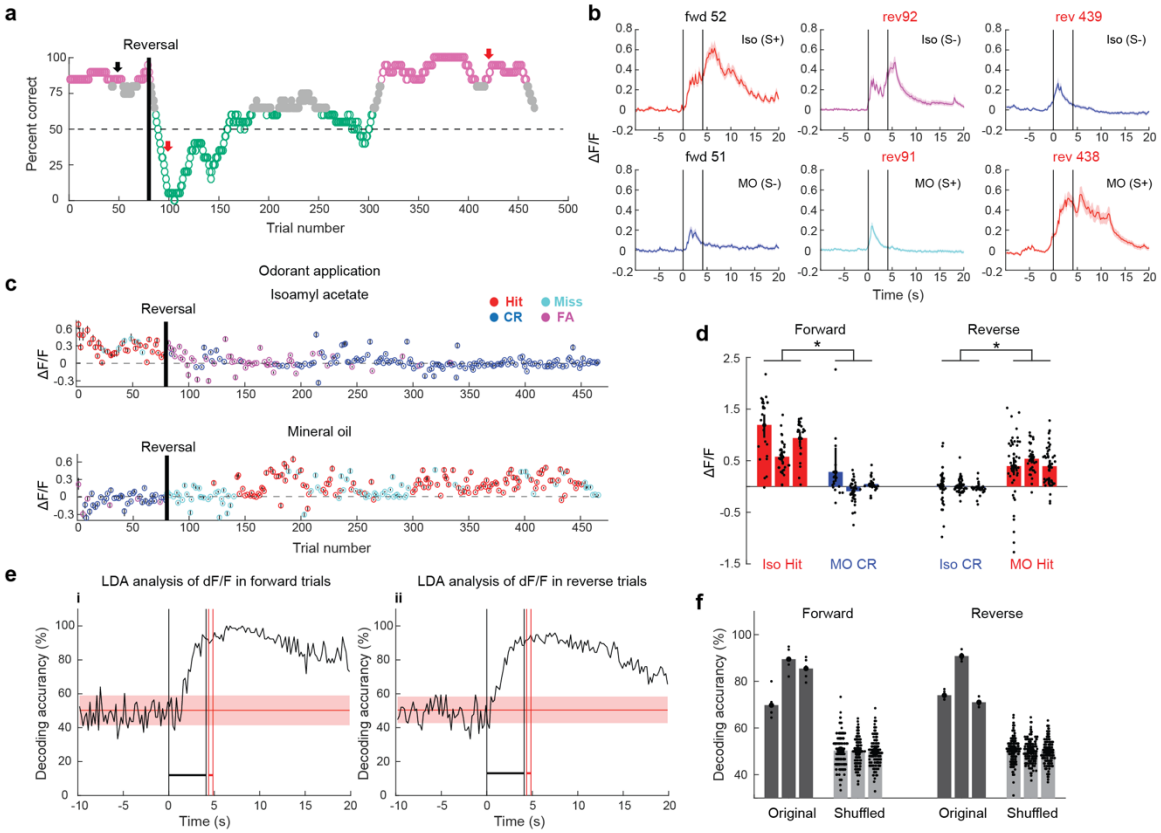

Figure 4. MLI odorant responses switched after reversal.

Panels **a-c and e** show behavioral performance (**a**), ΔF/F (**b** and **c**) and LDA analysis (**e**) for one session where odorant reinforcement was reversed (one mouse).

a. Learning curve showing the animal's behavior after reversal. Green <=65%, magenta: >=80% correct. Forward: S+ 1% Iso and S- MO.

b. Average ΔF/F time courses for example trials before (trials 51 and 52) and shortly after reversal (trials 91 and 92), and after the animal attained proficiency during reversal (trials 438 and 439). The vertical black lines are odorant onset and removal.

c. Per trial average ΔF/F during the last second of odorant application for the reversal task in Fig. 4a. The upper plot shows the responses to Iso and the lower plot shows responses to MO.

785 **d**. Odorant-induced changes in ΔF/F recorded from three animals computed for trials when
786 the animal was behaving >=80% correct. Vertical lines are 95% CIs. Red: Hit, Blue: CR.
787 A GLM analysis indicates that there is a significant difference in odor-induced changes in
788 ΔF/F for both odorant and reversal ($p<0.001$, 12 observations, 8 d.f., n=3 sessions, 3 mice,
789 GLM F-statistic=14.8, $p<0.01$).
790 **e**. Time course for decoding accuracy computed with LDA analysis of ΔF/F data for all
791 ROIs in the FOV. The shade is the 95% CI of decoding accuracy calculated with shuffled
792 odorant identity. The vertical black lines are odorant onset and removal and the red lines
793 bound the reinforcement period.
794 **f**. Decoding accuracy for three animals calculated with odorant-induced changes in ΔF/F
795 from trials where the animal was performing >=80% correct. Vertical lines are 95% CIs.
796 Dark-gray: original, light-gray: shuffled. A GLM analysis indicates that differences in
797 decoding accuracy are statistically significant between original and shuffled ($P<0.001$), but
798 not between forward and reverse ($p>0.05$, n=12, 8 d.f., n=3 sessions, 3 mice, GLM F-
799 statistic=16, $p<0.001$).
800
801
802

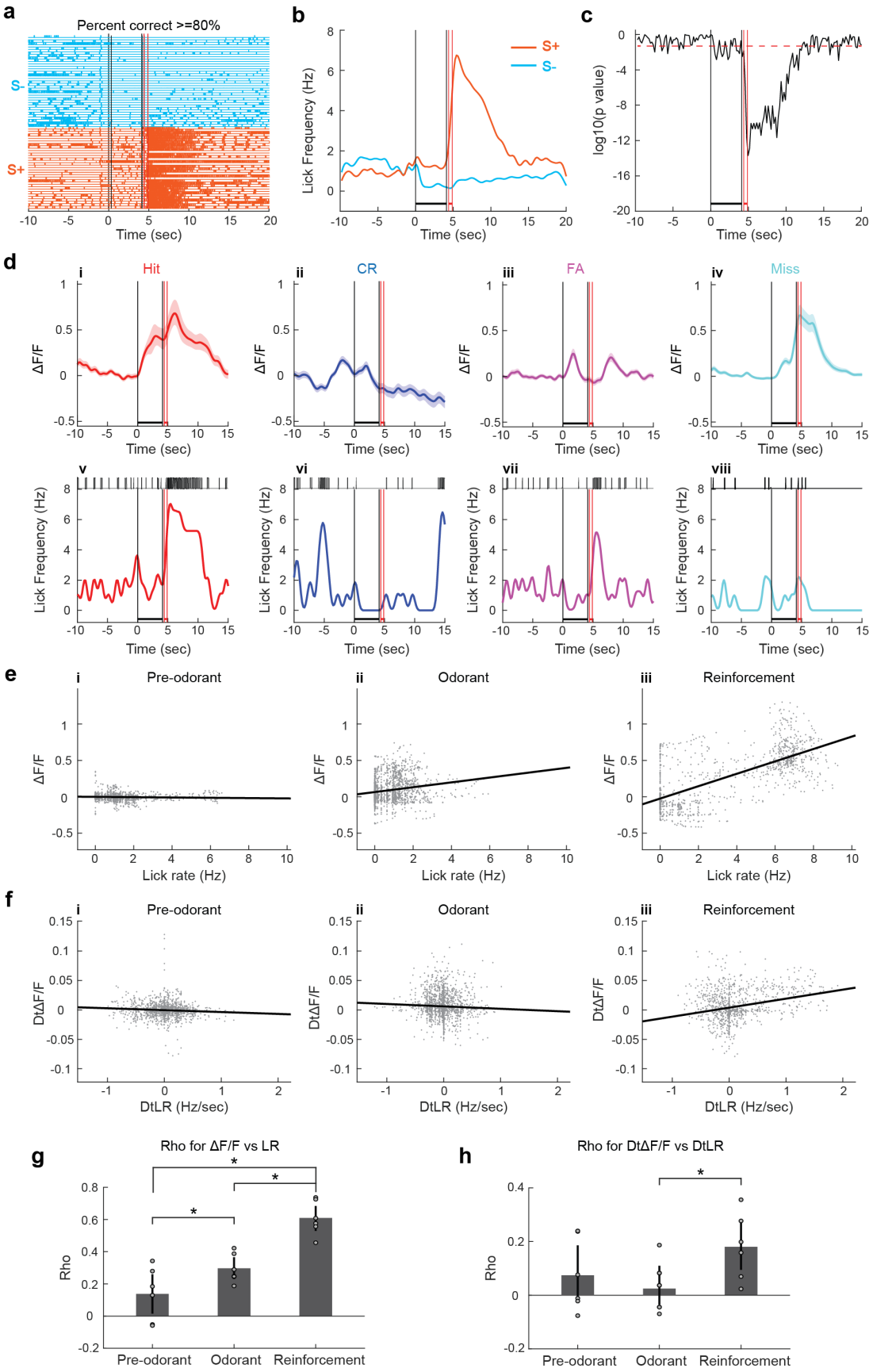
a
Percent correct >=80%
S-
S+
Time (sec)
b
Lick Frequency (Hz)
S+
S-
Time (sec)
c
log10(p value)
Time (sec)
d
i Hit
ii CR
iii FA
iv Miss
ΔF/F
Time (sec)
v
vi
vii
viii
Lick Frequency (Hz)
Time (sec)
e
i Pre-odorant
ii Odorant
iii Reinforcement
ΔF/F
Lick rate (Hz)
f
i Pre-odorant
ii Odorant
iii Reinforcement
DtΔF/F
DtLR (Hz/sec)
g
Rho for ΔF/F vs LR
Rho
Pre-odorant
Odorant
Reinforcement
h
Rho for DtΔF/F vs DtLR
Rho
Pre-odorant
Odorant
Reinforcement

803

804 **Figure 5. Changes in lick rate correlate with changes in MLI activity during the**
805 **reinforcement period, but not during the odorant period.**
806 Panels **a-d** are examples of lick traces (**a**), lick frequency (**b**), lick ranksum p value (**c**) and
807 ΔF/F (**d**) for one session (one mouse).
808 **a**. Examples of per trial lick traces when the mouse was learning to discriminate the
809 odorants when the animal was proficient (>=80% correct, orange traces: S+ trials, light
810 blue traces: S- trials).
811 **b**. Average lick frequency for S+ (orange) and S- (light blue) trials shown in **a**.
812 **c**. p value for a ranksum test estimating the difference in licks between the S+ and S-
813 odorants for the example in **a**.
814 **d**. Single trial examples of average ΔF/F (±CI, shade, n=105 ROIs) (**i-iv**) and the
815 corresponding lick frequency and lick traces (**v-viii**).
816 **e**. Relationship between the per trial average ΔF/F and the lick frequency shown per time
817 point for all trials in a go-no go session (one session, one mouse). Time points are
818 segregated within the last second before odorant addition (Pre-odorant), during the last
819 second of odorant addition (Odorant) and during the 1.5 seconds after reward
820 (Reinforcement). Correlation coefficients and p values for these time periods are: Pre-
821 odorant: 0.058, $p<0.05$. Odorant: 0.19, $p<0.001$. Reinforcement: 0.73, $p<0.001$.
822 *p<pFDR=0.05, n=6 sessions, 5 mice.
823 **f**. Relationship between the derivative of average ΔF/F and the derivative of lick frequency
824 shown per time point for all trials in a go-no go session (one session, one mouse). Time
825 points are segregated within the last second before odorant addition (Pre-odorant), during
826 the last second of odorant addition (Odorant) and during 1.5 seconds after reward

827 (Reinforcement). Correlation coefficients and p values for these time periods are: Pre-
828 odorant: -0.076, $p<0.01$. Odorant: -0.045, $p>0.05$. Reinforcement: 0.28, $p<0.001$.
829 *$p<pFDR=0.016$, n=6 sessions, 5 mice.
830 **g**. Correlation coefficients for the relationship between the average ΔF/F and lick frequency
831 for six sessions (five mice). The correlation coefficient is significantly different between
832 reinforcement and odorant (*t test $p<pFDR=0.05$, n=6 sessions, 5 mice).
833 **h**. Correlation coefficients for the relationship between the derivative of average ΔF/F and
834 the derivative of lick frequency for six sessions (five mice). The correlation coefficient is
835 significantly different between reinforcement and odorant (*t test $p<pFDR=0.016$, n=6
836 sessions, 5 mice).
837 In b, c and d the vertical black lines are odorant onset and removal and the vertical red lines
838 bound the reinforcement period.
839 All data shown in this figure are for proficient mice (percent correct>=80%).
840
841
842
843

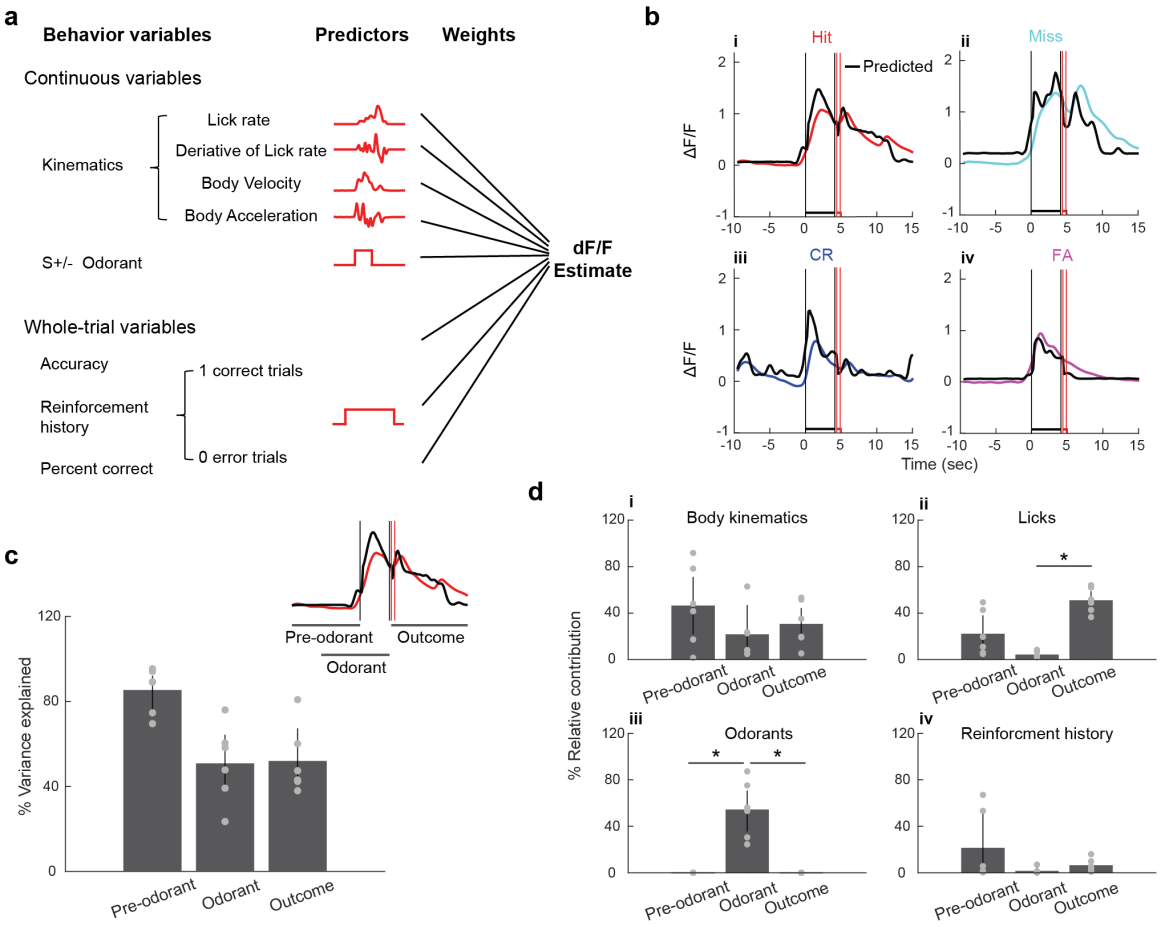

Figure 6. Fit of MLI activity with a generalized linear model

a. Schematic illustration of the variables used by the GLM model to quantify the relationship between average ΔF/F and behavioral variables and odorant valence on a per trial basis.

b. Examples of GLM best-fit (black) and actual ΔF/F Ca^{2+} traces for Hit (**i,** red), Miss (**ii**, cyan), CR (**iii**, blue) and FA (**iv**, magenta) trials. The vertical black lines are odorant onset and removal and the red lines bound the reinforcement period.

c. Percent of the variance explained by GLM in the different time periods (Pre-odorant, Odorant and Outcome). The inset shows the time intervals used for the different periods.

d. Relative contribution of kinematics (**i**), licks (**ii**), odorants (**iii**) and reinforcement history (**iv**) to the GLM fit for fits in the different time periods (pre-odorant, odorant, outcome). The results showed that odorants and licks play an important role in contributing to the activity during odorants and outcome periods respectively, while kinematics contribute to the activity in all three time periods. Asterisks for Licks (**ii**) and Odorants (**iii**) denote significant differences determined by ranksum and t test ($p<pFDR=0.033$, n=6 sessions, 5 mice). There are no significant differences for Kinematics (**i**) or Reinforcement history (**iv**) ($p>pFDR=0.017$, ranksum test).

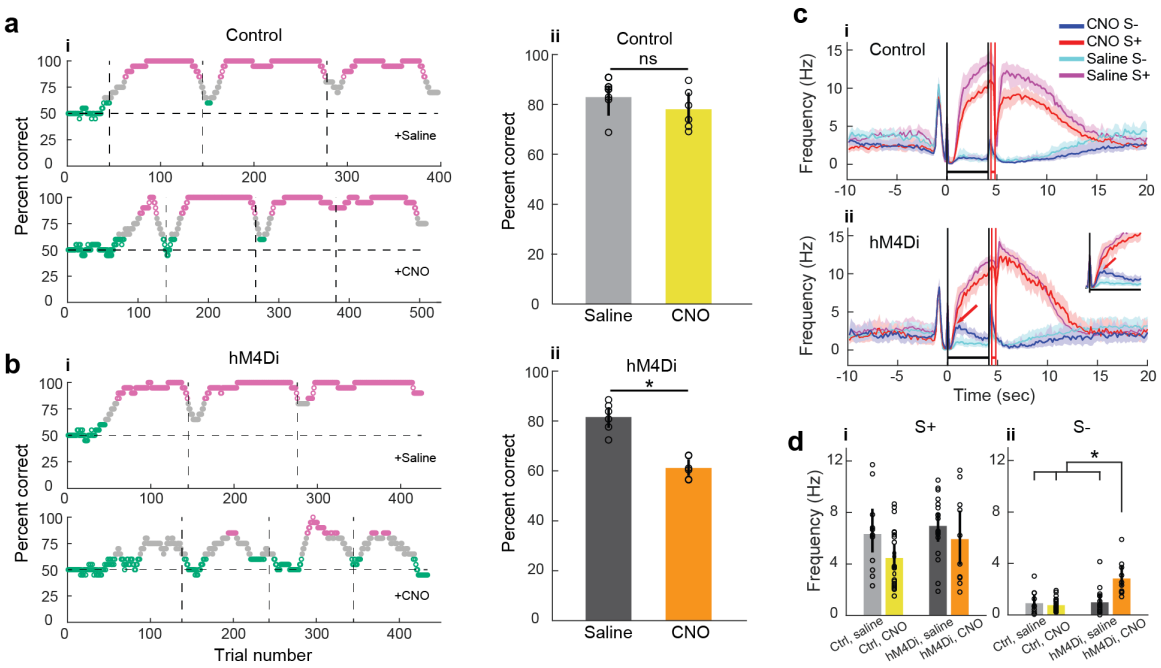

Figure 7. Chemogenetic inhibition of MLI activity impairs associative learning.

a. and b. a,i and b,i. Examples of behavioral performance in a go-no go task where mice learned to differentiate between two odorant mixtures (S+: 0.1% of 60% heptanal+40% ethyl butyrate, S-: 0.1% of 40% heptanal+60% ethyl butyrate). Green: <=65% correct, magenta: >=80% correct. The vertical lines are the boundaries between different daily sessions.

a,ii and b,ii. Behavioral performance (mean± 95% CIs, n=6). **a.** Mice expressing mCherry in MLIs (control mice). **b.** Mice expressing hM4Di in MLIs. A GLM analysis indicates that there is a statistically significant interaction between CNO drug treatment and hM4Di expression ($p<0.01$, 24 observations, 20 d.f., n=6 mice, GLM F-statistic=13.7, $p<0.001$) and post hoc unpaired t tests indicate that the hM4Di expressing group differs between CNO and saline (asterisks, $p<pFDR=0.025$, n=12 mice).

c. Average lick frequency time course for the control (**i**) and hM4Di (**ii**) groups (mean± 95% CI, shade). The arrow in the inset shows that for S- trials of CNO treated hM4Di

879 animals (blue), the animal kept licking for a longer time than S- trials for mice injected
880 with saline (cyan). The vertical black lines are odorant onset and removal and the red lines
881 bound the reinforcement period.
882 **d**. Mean lick frequency (±CI) during the initial portion of the odorant application period
883 (0.8 to 1.8 sec) for mice performing >=80% correct (**i**: S+, **ii**: S-). GLM analysis did not
884 find a statistically significant difference for treatment or hM4Di expression (or
885 interactions) for S+ ($p>0.05$, 60 observations, 56 d.f., n=6 mice, GLM F-statistic=2.96,
886 $p>0.05$), but found a difference for CNO treatment x hM4Di expression for S- ($p<0.001$,
887 60 observations, 56 d.f., n=6 mice, GLM F-statistic=12.8, $p<0.001$). *p<pFDR=0.03 for
888 post-hoc t-test.
889
890

1 Cayco-Gajic, N. A. & Silver, R. A. Re-evaluating Circuit Mechanisms Underlying Pattern Separation. *Neuron* **101**, 584-602, doi:10.1016/j.neuron.2019.01.044 (2019).

2 Strick, P. L., Dum, R. P. & Fiez, J. A. Cerebellum and nonmotor function. *Annu Rev Neurosci* **32**, 413-434, doi:10.1146/annurev.neuro.31.060407.125606 (2009).

3 Sokolov, A. A., Miall, R. C. & Ivry, R. B. The Cerebellum: Adaptive Prediction for Movement and Cognition. *Trends Cogn Sci* **21**, 313-332, doi:10.1016/j.tics.2017.02.005 (2017).

4 Adamaszek, M. *et al.* Consensus Paper: Cerebellum and Emotion. *Cerebellum* **16**, 552-576, doi:10.1007/s12311-016-0815-8 (2017).

5 Badura, A. *et al.* Normal cognitive and social development require posterior cerebellar activity. *Elife* **7**, doi:10.7554/eLife.36401 (2018).

6 Jelitai, M., Puggioni, P., Ishikawa, T., Rinaldi, A. & Duguid, I. Dendritic excitation-inhibition balance shapes cerebellar output during motor behaviour. *Nat Commun* **7**, 13722, doi:10.1038/ncomms13722 (2016).

7 Gao, Z., van Beugen, B. J. & De Zeeuw, C. I. Distributed synergistic plasticity and cerebellar learning. *Nat Rev Neurosci* **13**, 619-635, doi:10.1038/nrn3312 (2012).

8 Marr, D. A theory of cerebellar cortex. *J Physiol* **202**, 437-470 (1969).

9 Ito, M. Neural design of the cerebellar motor control system. *Brain Res* **40**, 81-84, doi:10.1016/0006-8993(72)90110-2 (1972).

10 Albus, J. S. A theory of cerebellar function. *Mathematical Biosciences* **10**, 25-61 (1971).

11 Heffley, W. & Hull, C. Classical conditioning drives learned reward prediction signals in climbing fibers across the lateral cerebellum. *Elife* **8**, doi:10.7554/eLife.46764 (2019).

12 Tsutsumi, S. *et al.* Modular organization of cerebellar climbing fiber inputs during goal-directed behavior. *Elife* **8**, doi:10.7554/eLife.47021 (2019).

13 Deverett, B., Koay, S. A., Oostland, M. & Wang, S. S. Cerebellar involvement in an evidence-accumulation decision-making task. *Elife* **7**, doi:10.7554/eLife.36781 (2018).

14 Carta, I., Chen, C. H., Schott, A. L., Dorizan, S. & Khodakhah, K. Cerebellar modulation of the reward circuitry and social behavior. *Science* **363**, doi:10.1126/science.aav0581 (2019).

15 Schonewille, M. *et al.* Reevaluating the role of LTD in cerebellar motor learning. *Neuron* **70**, 43-50, doi:10.1016/j.neuron.2011.02.044 (2011).

16 Dean, P., Porrill, J., Ekerot, C. F. & Jorntell, H. The cerebellar microcircuit as an adaptive filter: experimental and computational evidence. *Nat Rev Neurosci* **11**, 30-43, doi:10.1038/nrn2756 (2010).

930 17 Rancillac, A. & Crepel, F. Synapses between parallel fibres and stellate cells
931 express long-term changes in synaptic efficacy in rat cerebellum. *J Physiol* **554**,
932 707-720, doi:10.1113/jphysiol.2003.055871 (2004).

933 18 Liu, S. Q. & Cull-Candy, S. G. Synaptic activity at calcium-permeable AMPA
934 receptors induces a switch in receptor subtype. *Nature* **405**, 454-458,
935 doi:10.1038/35013064 (2000).

936 19 Jorntell, H. & Ekerot, C. F. Receptive field plasticity profoundly alters the
937 cutaneous parallel fiber synaptic input to cerebellar interneurons in vivo. *J Neurosci*
938 **23**, 9620-9631 (2003).

939 20 Jorntell, H. & Ekerot, C. F. Reciprocal bidirectional plasticity of parallel fiber
940 receptive fields in cerebellar Purkinje cells and their afferent interneurons. *Neuron*
941 **34**, 797-806, doi:10.1016/s0896-6273(02)00713-4 (2002).

942 21 Jorntell, H., Bengtsson, F., Schonewille, M. & De Zeeuw, C. I. Cerebellar
943 molecular layer interneurons - computational properties and roles in learning.
944 *Trends Neurosci* **33**, 524-532, doi:10.1016/j.tins.2010.08.004 (2010).

945 22 Liu, Y. *et al.* A single fear-inducing stimulus induces a transcription-dependent
946 switch in synaptic AMPAR phenotype. *Nat Neurosci* **13**, 223-231,
947 doi:10.1038/nn.2474 (2010).

948 23 Wulff, P. *et al.* Synaptic inhibition of Purkinje cells mediates consolidation of
949 vestibulo-cerebellar motor learning. *Nat Neurosci* **12**, 1042-1049,
950 doi:10.1038/nn.2348 (2009).

951 24 ten Brinke, M. M. *et al.* Evolving Models of Pavlovian Conditioning: Cerebellar
952 Cortical Dynamics in Awake Behaving Mice. *Cell Rep* **13**, 1977-1988,
953 doi:10.1016/j.celrep.2015.10.057 (2015).

954 25 Rowan, M. J. M. *et al.* Graded Control of Climbing-Fiber-Mediated Plasticity and
955 Learning by Inhibition in the Cerebellum. *Neuron* **99**, 999-1015 e1016,
956 doi:10.1016/j.neuron.2018.07.024 (2018).

957 26 Gire, D. H., Whitesell, J. D., Doucette, W. & Restrepo, D. Information for decision-
958 making and stimulus identification is multiplexed in sensory cortex. *Nat Neurosci*
959 **16**, 991-993, doi:10.1038/nn.3432 (2013).

960 27 Doucette, W. & Restrepo, D. Profound context-dependent plasticity of mitral cell
961 responses in olfactory bulb. *PLoS Biol* **6**, e258, doi:08-PLBI-RA-1962 [pii]

962 10.1371/journal.pbio.0060258 (2008).

963 28 Helmchen, F. & Denk, W. Deep tissue two-photon microscopy. *Nature methods* **2**,
964 932-940, doi:10.1038/nmeth818 (2005).

965 29 Giovannucci, A. *et al.* Cerebellar granule cells acquire a widespread predictive
966 feedback signal during motor learning. *Nat Neurosci* **20**, 727-734,
967 doi:10.1038/nn.4531 (2017).

968 30 Wagner, M. J., Kim, T. H., Savall, J., Schnitzer, M. J. & Luo, L. Cerebellar granule
969 cells encode the expectation of reward. *Nature* **544**, 96-100,
970 doi:10.1038/nature21726 (2017).

971 31 Giovannucci, A. *et al.* CaImAn an open source tool for scalable calcium imaging
972 data analysis. *Elife* **8**, doi:10.7554/eLife.38173 (2019).

973 32 Chu, C. P., Bing, Y. H., Liu, H. & Qiu, D. L. Roles of molecular layer interneurons
974 in sensory information processing in mouse cerebellar cortex Crus II in vivo. *PLoS*
975 *One* **7**, e37031, doi:10.1371/journal.pone.0037031 (2012).

976 33 Curran-Everett, D. Multiple comparisons: philosophies and illustrations.
977 *Am.J.Physiol Regul.Integr.Comp Physiol* **279**, R1-R8 (2000).

978 34 Gaffield, M. A. & Christie, J. M. Movement Rate Is Encoded and Influenced by
979 Widespread, Coherent Activity of Cerebellar Molecular Layer Interneurons. *J*
980 *Neurosci* **37**, 4751-4765, doi:10.1523/JNEUROSCI.0534-17.2017 (2017).

981 35 Astorga, G. *et al.* Concerted Interneuron Activity in the Cerebellar Molecular Layer
982 During Rhythmic Oromotor Behaviors. *J Neurosci* **37**, 11455-11468,
983 doi:10.1523/JNEUROSCI.1091-17.2017 (2017).

984 36 Tye, K. M. Neural Circuit Motifs in Valence Processing. *Neuron* **100**, 436-452,
985 doi:10.1016/j.neuron.2018.10.001 (2018).

986 37 Engelhard, B. *et al.* Specialized coding of sensory, motor and cognitive variables
987 in VTA dopamine neurons. *Nature* **570**, 509-513, doi:10.1038/s41586-019-1261-9
988 (2019).

989 38 Armbruster, B. N., Li, X., Pausch, M. H., Herlitze, S. & Roth, B. L. Evolving the
990 lock to fit the key to create a family of G protein-coupled receptors potently

991 activated by an inert ligand. *Proc Natl Acad Sci U S A* **104**, 5163-5168,
992 doi:10.1073/pnas.0700293104 (2007).

993 39 Gomez, J. L. *et al.* Chemogenetics revealed: DREADD occupancy and activation
994 via converted clozapine. *Science* **357**, 503-507, doi:10.1126/science.aan2475
995 (2017).

996 40 Raymond, J. L. & Medina, J. F. Computational Principles of Supervised Learning
997 in the Cerebellum. *Annu Rev Neurosci* **41**, 233-253, doi:10.1146/annurev-neuro-
998 080317-061948 (2018).

999 41 Davie, J. T., Clark, B. A. & Hausser, M. The origin of the complex spike in
1000 cerebellar Purkinje cells. *J Neurosci* **28**, 7599-7609,
1001 doi:10.1523/JNEUROSCI.0559-08.2008 (2008).

1002 42 Otsu, Y. *et al.* Activity-dependent gating of calcium spikes by A-type K+ channels
1003 controls climbing fiber signaling in Purkinje cell dendrites. *Neuron* **84**, 137-151,
1004 doi:10.1016/j.neuron.2014.08.035 (2014).

1005 43 Rancz, E. A. & Hausser, M. Dendritic calcium spikes are tunable triggers of
1006 cannabinoid release and short-term synaptic plasticity in cerebellar Purkinje
1007 neurons. *J Neurosci* **26**, 5428-5437, doi:10.1523/JNEUROSCI.5284-05.2006
1008 (2006).

1009 44 Eccles, J. C., Llinas, R. & Sasaki, K. The excitatory synaptic action of climbing
1010 fibres on the Purkinje cells of the cerebellum. *J Physiol* **182**, 268-296,
1011 doi:10.1113/jphysiol.1966.sp007824 (1966).

1012 45 Finch, E. A., Tanaka, K. & Augustine, G. J. Calcium as a trigger for cerebellar long-
1013 term synaptic depression. *Cerebellum* **11**, 706-717, doi:10.1007/s12311-011-0314-
1014 x (2012).

1015 46 Linden, D. J. & Connor, J. A. Long-term synaptic depression. *Annu Rev Neurosci*
1016 **18**, 319-357, doi:10.1146/annurev.ne.18.030195.001535 (1995).

1017 47 Brown, A. M. *et al.* Molecular layer interneurons shape the spike activity of
1018 cerebellar Purkinje cells. *Sci Rep* **9**, 1742, doi:10.1038/s41598-018-38264-1 (2019).

1019 48 Gaffield, M. A., Rowan, M. J. M., Amat, S. B., Hirai, H. & Christie, J. M. Inhibition
1020 gates supralinear Ca(2+) signaling in Purkinje cell dendrites during practiced
1021 movements. *Elife* **7**, doi:10.7554/eLife.36246 (2018).

1022 49 Jorntell, H. & Ekerot, C. F. Receptive Field Remodeling Induced by Skin
1023 Stimulation in Cerebellar Neurons in vivo. *Front Neural Circuits* **5**, 3,
1024 doi:10.3389/fncir.2011.00003 (2011).

1025 50 Lennon, W., Yamazaki, T. & Hecht-Nielsen, R. A Model of In vitro Plasticity at
1026 the Parallel Fiber-Molecular Layer Interneuron Synapses. *Front Comput Neurosci*
1027 **9**, 150, doi:10.3389/fncom.2015.00150 (2015).

1028 51 Szapiro, G. & Barbour, B. Multiple climbing fibers signal to molecular layer
1029 interneurons exclusively via glutamate spillover. *Nat Neurosci* **10**, 735-742,
1030 doi:10.1038/nn1907 (2007).

1031 52 Arlt, C. & Hausser, M. Microcircuit Rules Governing Impact of Single Interneurons
1032 on Purkinje Cell Output In Vivo. *Cell Rep* **30**, 3020-3035 e3023,
1033 doi:10.1016/j.celrep.2020.02.009 (2020).

1034 53 Bing, Y. H., Wu, M. C., Chu, C. P. & Qiu, D. L. Facial stimulation induces long-
1035 term depression at cerebellar molecular layer interneuron-Purkinje cell synapses in
1036 vivo in mice. *Front Cell Neurosci* **9**, 214, doi:10.3389/fncel.2015.00214 (2015).

1037 54 Chabrol, F. P., Blot, A. & Mrsic-Flogel, T. D. Cerebellar Contribution to
1038 Preparatory Activity in Motor Neocortex. *Neuron* **103**, 506-519 e504,
1039 doi:10.1016/j.neuron.2019.05.022 (2019).

1040 55 Hernandez-Briones, Z. S. *et al.* Olfactory stimulation induces cerebellar vermis
1041 activation during sexual learning in male rats. *Neurobiol Learn Mem* **146**, 31-36,
1042 doi:10.1016/j.nlm.2017.11.003 (2017).

1043 56 Sobel, N. *et al.* Odorant-induced and sniff-induced activation in the cerebellum of
1044 the human. *J Neurosci* **18**, 8990-9001 (1998).

1045 57 Mainland, J. D., Johnson, B. N., Khan, R., Ivry, R. B. & Sobel, N. Olfactory
1046 impairments in patients with unilateral cerebellar lesions are selective to inputs
1047 from the contralesional nostril. *J Neurosci* **25**, 6362-6371,
1048 doi:10.1523/JNEUROSCI.0920-05.2005 (2005).

1049 58 Kostadinov, D., Beau, M., Blanco-Pozo, M. & Hausser, M. Predictive and reactive
1050 reward signals conveyed by climbing fiber inputs to cerebellar Purkinje cells. *Nat*
1051 *Neurosci* **22**, 950-962, doi:10.1038/s41593-019-0381-8 (2019).

1052 59 Heffley, W. *et al.* Coordinated cerebellar climbing fiber activity signals learned
1053 sensorimotor predictions. *Nat Neurosci* **21**, 1431-1441, doi:10.1038/s41593-018-
1054 0228-8 (2018).

1055 60 Vincent, P. & Marty, A. Fluctuations of inhibitory postsynaptic currents in Purkinje
1056 cells from rat cerebellar slices. *J Physiol* **494 (Pt 1)**, 183-199,
1057 doi:10.1113/jphysiol.1996.sp021484 (1996).

1058 61 Palay, S. L. & Chan-Palay, V. *Cerebellar Cortex: Cytology and Organization*.
1059 (Springer Berlin Heidelberg, 1973).

1060 62 Dean, H. L., Hagan, M. A. & Pesaran, B. Only coherent spiking in posterior parietal
1061 cortex coordinates looking and reaching. *Neuron* **73**, 829-841,
1062 doi:10.1016/j.neuron.2011.12.035 (2012).

1063 63 Chen, T. W. *et al.* Ultrasensitive fluorescent proteins for imaging neuronal activity.
1064 *Nature* **499**, 295-300, doi:10.1038/nature12354 (2013).

1065 64 Astorga, G. *et al.* An excitatory GABA loop operating in vivo. *Front Cell Neurosci*
1066 **9**, 275, doi:10.3389/fncel.2015.00275 (2015).

1067 65 Kuhn, B., Ozden, I., Lampi, Y., Hasan, M. T. & Wang, S. S. An amplified promoter
1068 system for targeted expression of calcium indicator proteins in the cerebellar cortex.
1069 *Front Neural Circuits* **6**, 49, doi:10.3389/fncir.2012.00049 (2012).

1070 66 Li, A., Gire, D. H. & Restrepo, D. Y spike-field coherence in a population of
1071 olfactory bulb neurons differentiates between odors irrespective of associated

outcome. *J Neurosci* **35**, 5808-5822, doi:10.1523/JNEUROSCI.4003-14.2015 (2015).

67 Farneback, G. Two-frame motion estimation based on polynomial expansion. *Proceedings of the 13th Scandinavian Conference on Image Analysis*, 363-370 (2003).

68 Barnett, L. M., Hughes, T. E. & Drobizhev, M. Deciphering the molecular mechanism responsible for GCaMP6m's Ca2+-dependent change in fluorescence. *PLoS One* **12**, e0170934, doi:10.1371/journal.pone.0170934 (2017).

69 Litwin-Kumar, A., Harris, K. D., Axel, R., Sompolinsky, H. & Abbott, L. F. Optimal Degrees of Synaptic Connectivity. *Neuron* **93**, 1153-1164 e1157, doi:10.1016/j.neuron.2017.01.030 (2017).